This article has been accepted for inclusion in a future issue of this journal. Content is final as presented, with the exception of pagination.

Force-Sensor-Less Bilateral Teleoperation Control of Dissimilar Master–Slave System With Arbitrary Scaling

Santeri Lampinen, Janne Koivumäki, *Member, IEEE*, Wen-Hong Zhu, *Senior Member, IEEE*, and Jouni Mattila, *Member, IEEE*

***Abstract*— This study designs a high-precision bilateral teleoperation control for a dissimilar master–slave system. The proposed nonlinear control design takes advantage of a novel subsystem-dynamics-based control method that allows designing of individual (decentralized) model-based controllers for the manipulators locally at the subsystem level. Very importantly, a dynamic model of the human operator is incorporated into the control of the master manipulator. The individual controllers for the dissimilar master and slave manipulators are connected in a specific communication channel for the bilateral teleoperation to function. Stability of the overall control design is rigorously guaranteed with arbitrary time delays. Novel features of this study include the completely force-sensor-less design for the teleoperation system with a solution for a uniquely introduced computational algebraic loop, a method of estimating the exogenous operating force of an operator and the use of a commercial haptic manipulator. Most importantly, we conduct experiments on a dissimilar system in two degrees of freedom (DOFs). As an illustration of the performance of the proposed system, a force scaling factor of up to 800 and position scaling factor of up to 4 was used in the experiments. The experimental results show an exceptional tracking performance, verifying the real-world performance of the proposed concept.**

***Index Terms*— Contact force estimation, motion/force control, nonlinear control, stability, teleoperation, telerobotics.**

NOMENCLATURE

$(\cdot)_\gamma$	Subscript indicating whether the attribute refers to the master ($\gamma = m$) or the slave ($\gamma = s$).
$\Theta_m \in \mathbb{R}^{30\times 2}$	Mapping matrix.
$\dot{\mathbf{q}}_m \in \mathbb{R}^2$	Independent joint velocity coordinates of the master manipulator.
$\mathcal{V}_\gamma \in \mathbb{R}^2$	Velocity of the master/slave manipulator.
$\mathcal{V}_{\gamma r} \in \mathbb{R}^2$	Required counterpart of $\mathcal{V}_\gamma$.
$\mathcal{V}_{\gamma d} \in \mathbb{R}^2$	Desired counterpart of $\mathcal{V}_\gamma$.
$\mathcal{P}_\gamma \in \mathbb{R}^2$	Control point position of the manipulator.
$\mathbf{J}_m \in \mathbb{R}^{2\times 2}$	Jacobian matrix.
$\Phi_m \in \mathbb{R}^{30\times 2}$	Mapping matrix.
$M_m^* \in \mathbb{R}^{30\times 30}$	Equivalent inertial matrix.
$C_m^* \in \mathbb{R}^{30\times 30}$	Skew-symmetric matrix of the centrifugal and Coriolis terms.
$G_m^* \in \mathbb{R}^{30}$	Gravitation vector.
$\boldsymbol{\tau}_m \in \mathbb{R}^2$	Applied torques of the master manipulator.
$\boldsymbol{\tau}_{mm} \in \mathbb{R}^2$	Estimated dynamics of the master manipulator.
$\mathbf{f}_\gamma \in \mathbb{R}^2$	Contact force of the master/slave manipulator.
$\mathbf{A} \in \mathbb{R}^{2\times 2}$	Diagonal positive-definite matrix defining the gain of the force feedback.
$\mathbf{C} \in \mathbb{R}^{2\times 2}$	Diagonal positive-definite matrix defining the time constant of the first-order filter.
$\boldsymbol{\Lambda} \in \mathbb{R}^{2\times 2}$	Diagonal positive-definite matrix defining the gain of the position feedback.
$K_m \in \mathbb{R}^{2\times 2}$	Diagonal positive-definite matrix defining the gain of the internal velocity feedback.
$\kappa_f \in \mathbb{R}$	Force scaling factor.
$\kappa_p \in \mathbb{R}$	Position scaling factor.
$T \in \mathbb{R}$	Length of the one-way time delay.
$\sigma_f \in \{0, 1\}$	Selective factor to detect contact motion.

Tilde ($\tilde{}$) on top of a variable implies that the variable is filtered with a first-order filter, unless explicitly specified otherwise. Hat ($\hat{}$) on top of a variable implies that the variable is an estimate of itself, while wide hat ($\widehat{}$) is used to denote adapted parameters.

I. INTRODUCTION

BILATERALLY teleoperated robotic systems can bring the perception and precision of direct manipulation into challenging and risk-intensive tasks in environments that may be hazardous or hostile for humans. In contrast to unilateral teleoperation where the command flow goes only from the master to the slave, bilateral teleoperation provides the operator with information about the slave manipulator in the form of force feedback, to assist in the coordination and decision-making processes. To broaden the application scope of teleoperation,

Manuscript received December 2, 2020; revised March 23, 2021; accepted June 4, 2021. Manuscript received in final form June 18, 2021. This work was supported by the Finnish Foundation for Technology Promotion. Recommended by Associate Editor W. He. *(Corresponding author: Santeri Lampinen.)*

This work did not involve human subjects or animals in its research.

Santeri Lampinen, Janne Koivumäki, and Jouni Mattila are with the Faculty of Engineering and Natural Sciences, Tampere University, 33720 Tampere, Finland (e-mail: santeri.lampinen@tuni.fi; janne.koivumäki@tuni.fi; jouni.mattila@tuni.fi).

Wen-Hong Zhu is with the Canadian Space Agency, Longueuil (Saint-Hubert), QC J3Y 8Y9, Canada (e-mail: wenhong.zhu@canada.ca).

Color versions of one or more figures in this article are available at https://doi.org/10.1109/TCST.2021.3091314.

Digital Object Identifier 10.1109/TCST.2021.3091314

This work is licensed under a Creative Commons Attribution 4.0 License. For more information, see https://creativecommons.org/licenses/by/4.0/

This article has been accepted for inclusion in a future issue of this journal. Content is final as presented, with the exception of pagination.

arbitrary motion and forces scaling has been pursued by many researchers, but no rigorously stability guaranteed method has been shown to work in a multidegrees of freedom (DOF) system.

Currently, one of the most interesting applications for teleoperation lies in learning from demonstrations (LfD) applications with heavy-duty manipulators. LfD is an established technique in robotics, where a robot is taught to perform tasks by demonstrations from a human teacher. The robot can then repeat these tasks in even slightly varying conditions [1]. The *key enabler* for LfD applications with heavy-duty manipulators is teleoperation of asymmetric systems with *motion* and *force scaling*. Conventional kinesthetic teaching methods, established methods for providing teaching samples, cannot be applied to such manipulators due to the size and force limitations (workspace over 2 m and payload over 500 kg) [2]. Instead, teaching samples can be captured using teleoperation with motion and force scaling between the manipulators. Teleoperation has the advantage of an intuitive and efficient communication and operation strategy between humans and robots. Teleoperated demonstrations have been successfully used for LfD applications with promising results using 1:800 force scaling in [2], and using 1:1 scaling in [3] and [4].

In applications where heavy objects are handled or a great amount of force is required, hydraulic actuation has remained the most attractive solution due to its great power-to-weight ratio. Furthermore, hydraulic actuators have the benefits of simplicity, robustness, and low cost. However, control of such actuators is significantly challenged by their complex nonlinear dynamic behavior. When the actuators are used in articulated systems, the control design is further complicated by the associated nonlinear multibody dynamics, and the overall dynamics can be described by coupled nonlinear third-order differential equations. Consequently, the constrained motion control of multiple degrees-of-freedom (n-DOF) hydraulic robotic manipulators has been a well-recognized challenge [5]. As an additional challenge to the above, direct contact force measurements are usually used in contact control. In conventional applications, a 6-DOF force/torque sensor is often attached to the tip of the manipulator for this purpose. However, these force/torque sensors are expensive and prone to overloading and shocks, a situation frequently occurring with hydraulic heavy-duty manipulators [6]. Therefore, methods avoiding direct contact force measurements have become desirable.

Needless to say, teleoperation of hydraulic manipulators has been an extremely difficult problem due to unresolved challenges in their high-precision control [7]–[10]. However, due to recent state-of-the-art improvements and advances in high-precision control of hydraulic manipulators (see [5], [6], [11], [12]), their advanced teleoperation is suddenly becoming a feasible and interesting field of study again. Moreover, *time delay* (a focused research topic, especially in the teleoperation of extraterrestrial systems [13]) can be alternatively addressed for terrestrial applications in the advent of 5G cellular networks with ultralow latencies [14]. Such terrestrial applications are within the authors' main scope.

In contrast to a dissimilar master–slave configuration in Fig. 1, the current state of the art in teleoperation control has been mainly focusing on electrical manipulators in symmetrical 1:1 scale configurations, including multimaster or multislave setups, shared control, or dealing with time delays [15]–[20]. The existing methods for teleoperation of hydraulic manipulators have mainly relied on linear control theory and system linearization [8]–[10], [21]. However, these methods have limitations in teleoperation of complex, highly nonlinear, and asymmetric systems. In contrast, the adaptive teleoperation scheme proposed by Zhu and Salcudean in [22] was reported to be capable of addressing nonlinear dynamics of asymmetric master and slave manipulators with arbitrary motion and force scaling. However, experiments with only a 1-DOF symmetrical system were presented. Moreover, both manipulators were equipped with force sensors. Very recently, asymmetric teleoperation with motion scaling was discussed in [20], where a shared autonomy control strategy was proposed for handling redundant DOFs of the slave manipulator. Transparency was not considered in this study. Another recent approach for teleoperation of symmetric systems with varying time-delay was proposed in [19], where independent controllers were designed for both manipulators. The study demonstrated good transparency performance in constrained motion despite varying time delay, but lacked the ability to maintain transparency during transitions from free space motion to contact control.

A. Aim and Contribution

In this work, we target an asymmetric bilateral teleoperation system comprised of a commercial haptic master manipulator and a hydraulic slave manipulator. The system has notable asymmetry between the manipulators due to substantial differences between the dynamics of the master and slave manipulators. Due to this asymmetry, handling motion and force scaling in the teleoperation architecture becomes necessary. The studied system is shown in a high level in Fig. 1. The control design takes advantage of a novel subsystem-dynamics-based control method (see Section I-B) that enables individual model-based control designs for the manipulators locally at the subsystem level. Very importantly, a dynamic model of the human operator is incorporated into the control of the master manipulator. The individual controllers for the dissimilar master and slave manipulators are connected in a specific communication channel for the bilateral teleoperation to function.

In this study, the results of [22] and [23] are used as the foundation for designing a theoretically sound high-precision bilateral teleoperation control for significantly asymmetric systems. In [23], preliminary attempts for full-dynamics-based bilateral teleoperation for an asymmetric hydraulic/electric system were demonstrated, while in [24], artificial constraints in the task space were implemented. However, in-depth stability analysis and theoretical discussions were not included in [23] nor in [24].

To improve the preliminary theory and control performance reported in [23], the following *distinguishable contributions* are demonstrated in this study:

This article has been accepted for inclusion in a future issue of this journal. Content is final as presented, with the exception of pagination.

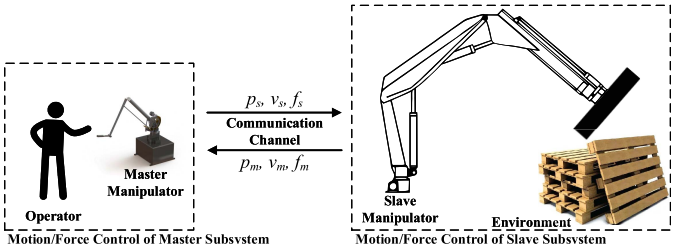

Fig. 1. High-level illustration of the studied dissimilar teleoperation system. A commercial haptic manipulator is used as the master manipulator, while a hydraulic loader crane complemented with a 500-kg dummy load at the TCP is used as the slave manipulator.

1) We propose a master manipulator contact force estimation by using joint control torques and estimated manipulator dynamics. A solution to a computational algebraic loop formed around the actuation and force estimation is proposed.
2) We propose a novel method for estimating the exogenous force of the human operator.
3) Stability of the overall control design is rigorously guaranteed with transparency and robustness against an arbitrary time delay.

With the control theoretical developments described above, the experiments demonstrate significant improvements in relation to our preliminary study [23]. The experiments with a 2-DOF system with a force scaling ratio of up to 800 and a position scaling ratio of up to 4, in lieu of the 1-DOF experiments in [22], serve *a critical step toward practical 6-DOF applications*.

B. Concept of the Virtual Decomposition Control

In modern control systems engineering, *modularity* is considered as a key aspect to address the ever-growing complexity of target applications [25]. To design the intended high-precision teleoperation for complex asymmetric system, the study takes advantage of a novel virtual decomposition control (VDC) approach (see [26], [27]). The method is developed especially for controlling complex robotic systems, with a number of significant state-of-the-art control performance improvements with robotic systems (see [5], [6], [11], [12], [22], [23], [28]). As a key feature, VDC enables to *virtually* break down complexity of the original system to a set of manageable *modular subsystems* [26], [28] such that the control design and stability analysis can be performed *locally at the subsystem level* without imposing additional approximations. This allows, for example, that *changing the control (or dynamics) of a subsystem does not affect the control equations of the rest of the system* [26].

The subsystem-dynamics-based control design philosophy in VDC originates from two unique concepts, namely *virtual stability* and *virtual power flows* (VPFs) (see Appendix B). The VPFs uniquely define the dynamic interactions among the subsystems such that the *virtual stability* of every subsystem ensures that a positive VPF is connected to its corresponding negative VPF in the adjacent subsystem (and vice versa). Thus, when every subsystem qualify as *virtually stable*, all the VPFs cancel each other out, eventually, leading to the stability of the entire system in the sense of Lebesgue integrable functions (see Appendix A). For more detailed information and additional benefits of VDCs, see [5] and [26].

C. Organization of the Article

The rest of this article is organized as follows: Section II presents the mathematical preliminaries. Section III discusses control of the master manipulator, while Section IV discusses control of the slave manipulator. Section V presents the teleoperation scheme and discusses properties of the teleoperation method. Section VI presents the experimental system and results. Finally, conclusions are drawn in Section VII.

II. Mathematical Preliminaries

Let an orthogonal coordinate system (i.e., a frame) $\{\mathbf{A}\}$ be attached to a rigid body. Then, the linear/angular velocity vector ${}^{\mathbf{A}}V \in \mathbb{R}^6$ and the force/moment vector ${}^{\mathbf{A}}F \in \mathbb{R}^6$ of the rigid body, expressed in frame $\{\mathbf{A}\}$, can be expressed as [26]

$$ {}^{\mathbf{A}}V = [{}^{\mathbf{A}}\mathbf{v} \quad {}^{\mathbf{A}}\boldsymbol{\omega}]^T, \quad {}^{\mathbf{A}}F = [{}^{\mathbf{A}}\mathbf{f} \quad {}^{\mathbf{A}}\mathbf{m}]^T $$

where ${}^{\mathbf{A}}\mathbf{v} \in \mathbb{R}^3$ and ${}^{\mathbf{A}}\boldsymbol{\omega} \in \mathbb{R}^3$ are the linear and angular velocity vectors of frame $\{\mathbf{A}\}$, expressed in frame $\{\mathbf{A}\}$, and ${}^{\mathbf{A}}\mathbf{f} \in \mathbb{R}^3$ and ${}^{\mathbf{A}}\mathbf{m} \in \mathbb{R}^3$ are the force and moment vectors that are being measured and expressed in frame $\{\mathbf{A}\}$, respectively.

Transformation of linear/angular and force/moment vectors between two frames, attached to a common rigid body, namely $\{\mathbf{A}\}$ and $\{\mathbf{B}\}$, can be expressed as [26]

$$ {}^{\mathbf{B}}V = {}^{\mathbf{A}}\mathbf{U}_{\mathbf{B}}^T \, {}^{\mathbf{A}}V \tag{1} $$

$$ {}^{\mathbf{A}}F = {}^{\mathbf{A}}\mathbf{U}_{\mathbf{B}} \, {}^{\mathbf{B}}F \tag{2} $$

where ${}^{\mathbf{A}}\mathbf{U}_{\mathbf{B}} \in \mathbb{R}^{6\times6}$ is a force/moment transformation matrix that also transform velocities between frames $\{\mathbf{A}\}$ and $\{\mathbf{B}\}$.

The dynamics of a freely moving rigid body, expressed in the fixed rigid body frame $\{\mathbf{A}\}$, can be defined as

$$ \mathbf{M}_{\mathbf{A}} \frac{d}{dt}({}^{\mathbf{A}}\mathbf{V}) + \mathbf{C}_{\mathbf{A}}({}^{\mathbf{A}}\omega) {}^{\mathbf{A}}\mathbf{V} + \mathbf{G}_{\mathbf{A}} = {}^{\mathbf{A}}F^* \tag{3} $$

where $\mathbf{M}_{\mathbf{A}} \in \mathbb{R}^{6\times6}$ is the mass matrix, $\mathbf{C}_{\mathbf{A}} \in \mathbb{R}^{6\times6}$ the Coriolis and centrifugal terms, and $\mathbf{G}_{\mathbf{A}} \in \mathbb{R}^{\mathbf{6}}$ the gravity vector of the rigid body. For a detailed formulation of $\mathbf{M}_{\mathbf{A}}$, $\mathbf{C}_{\mathbf{A}}$, and $\mathbf{G}_{\mathbf{A}}$, readers are referred to [26].

III. Master Manipulator

Phantom premium 3.0/6DOF, a commercial haptic manipulator without any modifications to the hardware, has been chosen to act as the master manipulator in this study. It possesses 6-DOF manipulability and force feedback along each individual DOF, with a workspace mimicking human arm motion pivoting from the shoulder. For this study, we developed a new control system for the manipulator to rigorously address the dynamics of the lightweight manipulator. As a challenge to the control design, the manipulator lacks force/torque sensors. Therefore, human operator contact force estimation is required. Without loss of generality, we consider manipulation and force perception only within a specific 2-DOF plane (by

This article has been accepted for inclusion in a future issue of this journal. Content is final as presented, with the exception of pagination.

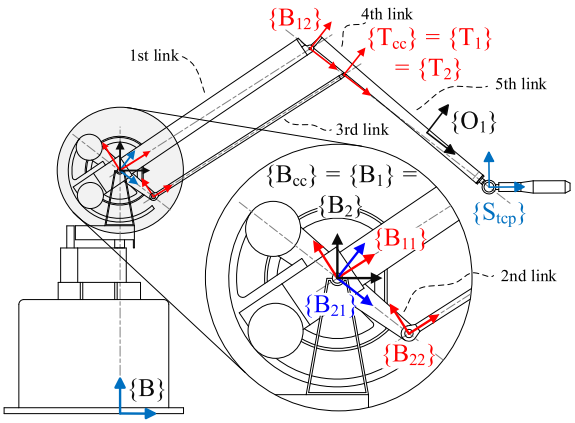

Fig. 2. Frame assignment of the haptic manipulator.

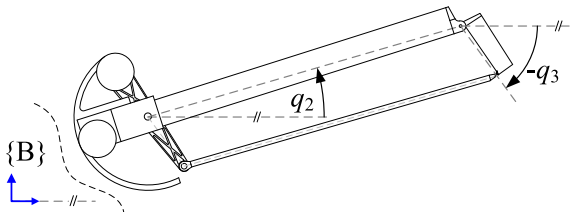

Fig. 3. Illustration of the joint angles of the master manipulator.

using joint 2 and joint 3), while the rest of the DOFs are locked with software. The benefit of using a commercial haptic device as the master manipulator is the ease of implementation for wide range of applications.

Frame $\{\mathbf{S_{tcp}}\}$ is assigned to the tool center point (TCP) of the master manipulator (see Fig. 2), and the external forces resulting from the dynamics of the human operator as well as the exogenous operating hand force are estimated and expressed in this frame. Orientation of frame $\{\mathbf{S_{tcp}}\}$ is aligned with the handle of the master manipulator and the handle is held horizontally as shown in Fig. 2 by position control at the spherical wrist.

A. Kinematics

Relevant coordinate frames in terms of control of the master manipulator are shown in Fig. 2. Notably, frame $\{\mathbf{B}_{11}\}$ is attached to the first link of the manipulator, $\{\mathbf{B}_{21}\}$ to the second link, $\{\mathbf{B}_{22}\}$ to the third link, $\{\mathbf{B}_{12}\}$ to the fourth link, and $\{\mathbf{O}_1\}$ to the fifth link. Numbering of the manipulator links is defined in Fig. 2.

Remark 1: Links 4 and 5 are virtually cut from the same rigid body, using design principles of the VDC approach, which allows separate computations later.

The independent joint velocity coordinates are denoted as

$$\dot{\mathbf{q}}_m = [\dot{q}_2 \quad \dot{q}_3]^T \in \mathbb{R}^2. \tag{4}$$

The respective joint angles q_2 and q_3 are shown in Fig. 3. Then, velocities of all links of the master manipulator can be determined using the geometrical transformation matrices between each frame with the independent joint velocity coordinates as

$$\mathbf{V}_m = \Theta_m \dot{\mathbf{q}}_m \tag{5}$$

where $\mathbf{V}_m = \left[{}^{\mathbf{B_{11}}}V^T \ {}^{\mathbf{B_{12}}}V^T \ {}^{\mathbf{B_{21}}}V^T \ {}^{\mathbf{B_{22}}}V^T \ {}^{\mathbf{O_1}}V^T\right]^T \in \mathbb{R}^{30}$, and $\Theta_m \in \mathbb{R}^{30\times 2}$ is a mapping matrix defined as

$$\Theta_m = \begin{bmatrix} \mathbf{z} & \mathbf{0}_{6\times 1} \\ {}^{\mathbf{B_{11}}}\mathbf{U}^T_{\mathbf{B_{12}}}\mathbf{z} - \mathbf{z} & \mathbf{z} \\ \mathbf{0}_{6\times 1} & \mathbf{z} \\ \mathbf{z} & {}^{\mathbf{B_{21}}}\mathbf{U}^T_{\mathbf{B_{22}}}\mathbf{z} - \mathbf{z} \\ {}^{\mathbf{B_{12}}}\mathbf{U}^T_{\mathbf{O_1}}\left({}^{\mathbf{B_{11}}}\mathbf{U}^T_{\mathbf{B_{12}}}\mathbf{z} - \mathbf{z}\right) & {}^{\mathbf{B_{12}}}\mathbf{U}^T_{\mathbf{O_1}}\mathbf{z} \end{bmatrix} \tag{6}$$

where $\mathbf{z} = [0\ 0\ 0\ 0\ 0\ 1]^T \in \mathbb{R}^6$.

Let the independent velocity coordinates at master manipulator's handle be $\mathcal{V}_m \in \mathbb{R}^2$ subject to

$$\mathcal{V}_m = \mathbf{J}_m \dot{\mathbf{q}}_m \tag{7}$$

$$\mathbf{J}_m = [\boldsymbol{I}_{2\times 2} \quad \mathbf{0}_{2\times 4}]\,{}^{\mathbf{O_1}}\mathbf{U}^T_{\mathbf{S_{tcp}}}[\mathbf{0}_{6\times 24} \quad \boldsymbol{I}_{6\times 6}]\Theta_m \tag{8}$$

where $\mathbf{J}_m \in \mathbb{R}^{2\times 2}$ is the invertible Jacobian matrix of the master manipulator.

Then, another mapping matrix can be defined as

$$\Phi_m = \Theta_m \mathbf{J}_m^{-1}. \tag{9}$$

B. Dynamics

Dynamics of each rigid body of the master manipulator can be determined using (3) and (5). According to [29], and under Assumption 1, the dynamic model of the master manipulator can be expressed as

$$\Phi_m^T \mathcal{M}_m^* \frac{d}{dt}(\Phi_m \mathcal{V}_m) + \left(\Phi_m^T \mathcal{C}_m^* \Phi_m\right)\mathcal{V}_m + \Phi_m^T \mathcal{G}_m^* = \mathbf{J}_m^{-T}\boldsymbol{\tau}_m - \mathbf{f}_m \tag{10}$$

where $\mathbf{f}_m$ is the net reaction force from the master manipulator toward the human operator and will be defined later in more detail, $\boldsymbol{\tau}_m \in \mathbb{R}^2$ denotes the applied torques of the manipulator, and

$$\mathcal{M}_m^* = \mathrm{diag}\{\mathbf{M}_{\mathbf{B_{11}}}, \ \mathbf{M}_{\mathbf{B_{12}}}, \ \mathbf{M}_{\mathbf{B_{21}}}, \ \mathbf{M}_{\mathbf{B_{22}}}, \ \mathbf{M}_{\mathbf{O_1}}\} \tag{11}$$

$$\mathcal{C}_m^* = \mathrm{diag}\{\mathbf{C}_{\mathbf{B_{11}}}, \ \mathbf{C}_{\mathbf{B_{12}}}, \ \mathbf{C}_{\mathbf{B_{21}}}, \ \mathbf{C}_{\mathbf{B_{22}}}, \ \mathbf{C}_{\mathbf{O_1}}\} \tag{12}$$

$$\mathcal{G}_m^* = \left[\mathbf{G}^T_{\mathbf{B_{11}}}, \ \mathbf{G}^T_{\mathbf{B_{12}}}, \ \mathbf{G}^T_{\mathbf{B_{21}}}, \ \mathbf{G}^T_{\mathbf{B_{22}}}, \ \mathbf{G}^T_{\mathbf{O_1}}\right]^T. \tag{13}$$

Assumption 1: Bearing friction of all the revolute joints of the master manipulator is zero.

C. Human Operator

Based on literature [22], [30], and [31], sufficient accuracy for modeling the human operator can be achieved using a simple second-order linear time-invariant model. The following model is used here:

$$\mathbf{M}_h \ddot{\mathbf{x}}_h + \mathbf{D}_h \dot{\mathbf{x}}_h + \mathbf{K}_h \mathbf{x}_h = \mathbf{f}_m - \mathbf{f}_h^* \tag{14}$$

where $\mathbf{M}_h \in \mathbb{R}^{2\times 2}$, $\mathbf{D}_h \in \mathbb{R}^{2\times 2}$, and $\mathbf{K}_h \in \mathbb{R}^{2\times 2}$ are symmetric positive-definite matrices approximating the inertia, damping, and stiffness of the arm of the human operator, respectively, while $\mathbf{f}_m \in \mathbb{R}^2$, appeared first in (10), denotes the net force vector, exerted by the master manipulator toward the operator, and $\mathbf{f}_h^* \in \mathbb{R}^2$ denotes the exogenous force vector actively generated by the operator. The position of the arm of the operator is denoted by $\mathbf{x}_h \in \mathbb{R}^2$, while $\dot{\mathbf{x}}_h \in \mathbb{R}^2$ and $\ddot{\mathbf{x}}_h \in \mathbb{R}^2$

This article has been accepted for inclusion in a future issue of this journal. Content is final as presented, with the exception of pagination.

denote the first and second time-derivatives of the position vector, respectively, subject to $\dot{\mathbf{x}}_h = \mathcal{V}_m$.

In [16] and [32], it was suggested that the exogenous force of the operator could be estimated using a fast parameter adaptation function. This differs from the approach in [22], where a switching term with a constant force, instead of an estimate, was used to ensure stability. The precise expression of the exogenous force, denoted $\mathbf{f}_h^* \in \mathbb{R}^2$ in (14), would necessarily involve research on complex human motor neuron actions. In this article, we describe this exogenous force as a general linear-in-parameter form as

$$\mathbf{f}_h^* = \Psi(t)\mathbf{p} \tag{15}$$

where $\Psi(t)$ is a time-variant matrix and $\mathbf{p}$ is a parameter vector. We treat vector $\mathbf{p}$ as a constant by moving all time-variant properties into $\Psi(t)$.

Remark 2: Note that expression (15) is quite general. It covers the expressions used in [16] and [17], in which $\Psi(t) = 1$ are used. Most importantly, this expression takes the same form commonly used in neural networks, allowing flexible incorporation of basis radial functions into machine learning mechanisms. With more elegant design of $\Psi(t)$, for example, muscle activation measured by electromyography (EMG) could be used for the intent force modeling. A recent comprehensive attempt at human arm dynamics modeling has been proposed in [33]. By modeling the motion dynamics of the arm and using time-variant muscle activation measured by EMG as the time-variant part, the human arm can be modeled similar to any multibody series manipulator. The multibody dynamics of the human arm together with its numerous muscle groups, tendons, and other ligaments can be modeled in pursuit of higher precision for more critical applications, for example, teleoperated surgery.

D. Control of the Master Manipulator With a Human Operator

For accurate control of the master manipulator, dynamics of both the manipulator itself and the human operator need to be addressed together. The required control law must, therefore, define required contact force toward the human operator.

The estimated human operator exogenous force is written as

$$\hat{\mathbf{f}}_h^* = \Psi(t)\widehat{\mathbf{p}} \tag{16}$$

where $\widehat{\mathbf{p}}$ is an estimate of the parameter vector. The time-invariant parameters are estimated using the following parameter adaptation law as

$$\begin{aligned} \dot{\widehat{p}}_i &= \rho_i \, \kappa \, \Psi_i(t)(\mathcal{V}_{mr} - \mathcal{V}_m) \\ \kappa &= \begin{cases} 0, & \hat{p}_i \le \hat{p}_i^- \text{ and } \mathrm{s} \le 0 \\ 0, & \hat{p}_i \ge \hat{p}_i^+ \text{ and } \mathrm{s} \ge 0 \\ 1, & \text{otherwise} \end{cases} \end{aligned} \tag{17}$$

where $\widehat{p}_i$, $\widehat{p}_i^+$, and $\widehat{p}_i^-$ are the estimate of the ith element of the real time-invariant parameter vector $\mathbf{p} = [p_1, p_2, \ldots, p_i, \ldots]^T$ as well as its upper and lower bounds, respectively, ρ_i is the adaptation gain of the ith element of $\widehat{\mathbf{p}} = [\widehat{p}_1, \widehat{p}_2, \ldots, \widehat{p}_i, \ldots]^T$, $\Psi_i(t)$ denotes the ith column of the time-variant matrix $\Psi(t)$, and $\mathcal{V}_{mr} \in \mathbb{R}^2$ denotes the required velocity at the tip of the master manipulator, expressed in frame $\{\mathbf{S_{tcp}}\}$. The designed bounds of $\widehat{p}$ define the maximum operator forces and it is defined to match the application requirements.

In Section III-B, dynamics were calculated using the measured independent joint velocity vector $\dot{\mathbf{q}}_m$. However, since the proposed control method is velocity-based, we need to define the required velocities in Cartesian space. Let $\mathcal{V}_{md} \in \mathbb{R}^2$ be the desired velocity of the tip of the master manipulator, to be defined later in Section V. Then, the required velocity vector, $\mathcal{V}_{mr} \in \mathbb{R}^2$, is designed as

$$\mathcal{V}_{mr} = \mathcal{V}_{md} - \mathbf{A}\tilde{\hat{\mathbf{f}}}_m \tag{18}$$

where $\mathbf{A} \in \mathbb{R}^{2\times 2}$ is a diagonal positive-definite gain matrix, and $\tilde{\hat{\mathbf{f}}}_m$ denotes a filtered estimate of the net reaction force of the master manipulator obtained using

$$\dot{\tilde{\hat{\mathbf{f}}}}_m + \mathbf{C}\tilde{\hat{\mathbf{f}}}_m = \mathbf{C}\hat{\mathbf{f}}_m \tag{19}$$

where $\mathbf{C} \in \mathbb{R}^{2\times 2}$ is a diagonal positive-definite matrix, and $\hat{\mathbf{f}}_m \in \mathbb{R}^2$ is an estimate of $\mathbf{f}_m$. The specific form of $\hat{\mathbf{f}}_m$ is discussed in detail in Section III-E.

Compute

$$\dot{\mathbf{q}}_{mr} = \mathbf{J}_m^{-1}\mathcal{V}_{mr} \tag{20}$$

$$\mathbf{V}_{mr} = \Theta_m \dot{\mathbf{q}}_{mr} \tag{21}$$

where $\dot{\mathbf{q}}_{mr} \in \mathbb{R}^2$ denotes the required counterpart of $\dot{\mathbf{q}}_m$, and $\mathbf{V}_{mr} \in \mathbb{R}^{30}$ denotes the required counterpart of $\mathbf{V}_m$.

Remark 3: The second term on the right-hand side of (18) acts as a local force feedback term within the control design.

The linear parametrization of the required rigid body dynamics can be written according to [26] as

$$\mathbf{Y_A}\theta_\mathbf{A} \equiv \mathbf{M_A}\frac{d}{dt}({}^\mathbf{A}V_\mathrm{r}) + \mathbf{C_A}({}^\mathbf{A}\omega){}^\mathbf{A}V_\mathrm{r} + \mathbf{G_A}. \tag{22}$$

Interested reader is referred to the formulation of the regressor matrix $\mathbf{Y_A} \in \mathbb{R}^{6\times 13}$ and the parameter vector $\boldsymbol{\theta}_\mathbf{A} \in \mathbb{R}^{13}$ in [26]. Using $\mathbf{A} \in \{\mathbf{B_{11}}, \mathbf{B_{12}}, \mathbf{B_{21}}, \mathbf{B_{22}}, \mathbf{O_1}\}$, dynamics of each rigid body can be calculated with (22) as

$$\begin{aligned} \mathbf{Y}_m\boldsymbol{\theta}_m = [&(\mathbf{Y}_{\mathbf{B_{11}}}\theta_{\mathbf{B_{11}}})^T,\ (\mathbf{Y}_{\mathbf{B_{12}}}\theta_{\mathbf{B_{12}}})^T,\ (\mathbf{Y}_{\mathbf{B_{21}}}\theta_{\mathbf{B_{21}}})^T, \\ &(\mathbf{Y}_{\mathbf{B_{22}}}\theta_{\mathbf{B_{22}}})^T,\ (\mathbf{Y}_{\mathbf{O_1}}\theta_{\mathbf{O_1}})^T]^T \in \mathbb{R}^{30} \end{aligned} \tag{23}$$

Furthermore, dynamics of the human operator are calculated with a similar linear parametrization form as

$$\mathbf{Y}_h\boldsymbol{\theta}_h = \mathbf{M}_h\dot{\mathcal{V}}_\mathrm{mr} + \mathbf{D}_h\dot{\mathbf{x}}_h + \mathbf{K}_h\mathbf{x}_h. \tag{24}$$

Then, control equations for the master manipulator can be defined as

$$\mathbf{J}_m^{-T}\boldsymbol{\tau}_m = \Phi_m^T\mathbf{Y}_m\boldsymbol{\theta}_m + \mathbf{Y}_h\boldsymbol{\theta}_h + \hat{\mathbf{f}}_h^* + K_m(\mathcal{V}_{mr} - \mathcal{V}_m) \tag{25}$$

where $K_m \in \mathbb{R}^{2\times 2}$ is a positive-definite gain matrix. The last term in (25) is a velocity feedback term used to ensure the control stability.

This article has been accepted for inclusion in a future issue of this journal. Content is final as presented, with the exception of pagination.

E. Force Estimation

The net reaction force from the master manipulator toward the operator can be estimated using the known dynamics of the master manipulator as a base. This method is similar to the inverse dynamics-based estimation methods, described in [34]. The main difference here is that the estimated actuator torque and applied torque are calculated based on the inverse dynamics, yielding that the external force can be estimated in addition to the mere collision detection, possible with the simpler method. The force estimate can be expressed as

$$\hat{\mathbf{f}}_m = \mathbf{J}_m^{-T}(\boldsymbol{\tau}_m - \boldsymbol{\tau}_{mm}) \tag{26}$$

where $\boldsymbol{\tau}_m$ is the master robot control input defined in (25), and $\boldsymbol{\tau}_{mm}$ is the estimated master robot dynamics, defined as

$$\boldsymbol{\tau}_{mm} = \left(\Theta_m^T \mathcal{M}_m^* \Theta_m\right)\hat{\dot{\mathbf{q}}}_m + \left(\Theta_m^T \mathcal{C}_m^* \Theta_m + \Theta_m^T \mathcal{M}_m^* \dot{\Theta}_m\right)\hat{\mathbf{q}}_m + \Theta_m^T \mathcal{G}_m^* \tag{27}$$

where $\hat{\dot{\mathbf{q}}}_m$ and $\hat{\mathbf{q}}_m$ are estimates of $\ddot{\mathbf{q}}_m$ and $\dot{\mathbf{q}}_m$, respectively, obtained by differentiation from the measured joint angles $\mathbf{q}_m$.

F. Algebraic Loop and Computation Algorithms

The force estimate in the control law in (25) results in an algebraic loop that has to be addressed to ensure stability of the control system. This section defines required conditions to ensure stability of the algebraic loop.

Differentiating (18) and expressing $\dot{\mathcal{V}}_{mr}$ as an affine function of $\dot{\tilde{\mathbf{f}}}_m$ yields

$$\dot{\mathcal{V}}_{mr} = \mathbf{A}_1(t)\dot{\tilde{\mathbf{f}}}_m + \mathbf{B}_1(t) \tag{28}$$

where $\mathbf{A}_1(t) \in \mathbb{R}^{2\times 2}$ is a known matrix and $\mathbf{B}_1(t) = \dot{\mathcal{V}}_{md} \in \mathbb{R}^2$ is a known vector (which will be given in Section V), and $\dot{\tilde{\mathbf{f}}}_m \in \mathbb{R}^2$ is a vector to be specified later in this section.

Using (20) and (21), it follows from (22)–(26) that

$$\hat{\mathbf{f}}_m = \mathbf{J}_m^{-T}(\boldsymbol{\tau}_m - \boldsymbol{\tau}_{mm}) = \mathbf{A}_2(t)\mathbf{A}\dot{\tilde{\mathbf{f}}}_m + \mathbf{B}_2(t) \tag{29}$$

where $\mathbf{A}_2(t) \in \mathbb{R}^{2\times 2}$ is a known matrix and $\mathbf{B}_2(t) \in \mathbb{R}^2$ is a known vector. Then, it follows from (19) that

$$\dot{\tilde{\mathbf{f}}}_m = (\mathbf{C}\mathbf{A}_2(t)\mathbf{A})\dot{\tilde{\mathbf{f}}}_m + \mathbf{B}_3(t) \tag{30}$$

where $\mathbf{B}_3(t) \in \mathbb{R}^2$ is a known vector. The existence of a computational algebraic loop can be clearly seen in (30).

To ensure numerical stability, we must have

$$\max_{\sigma}(\mathbf{C}\mathbf{A}_2(t)\mathbf{A}) < 1. \tag{31}$$

This means that both $\mathbf{C}$ and $\mathbf{A}$ must be restricted.

Finally, $\dot{\tilde{\mathbf{f}}}_m$ can be computed from (30) as

$$\dot{\tilde{\mathbf{f}}}_m = [\mathbf{I}_{2\times 2} - (\mathbf{C}\mathbf{A}_2(t)\mathbf{A})]^{-1}\mathbf{B}_3(t). \tag{32}$$

Once $\dot{\tilde{\mathbf{f}}}_m$ is obtained, $\tilde{\mathbf{f}}_m$ in (18) can be computed using integration with $\dot{\tilde{\mathbf{f}}}_m(0) = 0$.

G. Stability

Substituting (25) and (14) into (10) yields

$$\Phi_m^T \mathcal{M}_m^* \frac{d}{dt}(\Phi_m(\mathcal{V}_m - \mathcal{V}_{mr})) + M_h(\dot{\mathcal{V}}_m - \dot{\mathcal{V}}_{mr}) = \left(\Phi_m^T \mathcal{C}_m^* + K_m\right)(\mathcal{V}_{mr} - \mathcal{V}_m) + \Psi(t)(\hat{\mathbf{p}} - \mathbf{p}). \tag{33}$$

Next, the non-negative function for the master manipulator is chosen as

$$v_m = \frac{1}{2}(\mathcal{V}_{mr} - \mathcal{V}_m)^T\left(\Phi_m^T \mathcal{M}_m^* \Phi_m + M_h\right)(\mathcal{V}_{mr} - \mathcal{V}_m) + \frac{1}{2}\sum_i \frac{p_i - \hat{p}_i}{\rho_i}. \tag{34}$$

The time-derivative of the non-negative function in (34) is obtained using (33), (17), and the skew-symmetric properties of $\mathcal{C}_m^*$ as

$$\dot{v}_m \le -(\mathcal{V}_{mr} - \mathcal{V}_m)^T K_m(\mathcal{V}_{mr} - \mathcal{V}_m). \tag{35}$$

Theorem 1: Analyzing the master manipulator (10) with the human operator (14) subject to control (25) with estimated exogenous operator force using adaptation law (17), it yields

$$\xi_m \equiv \mathcal{V}_{md} - \mathcal{V}_m - \mathbf{A}\tilde{\hat{\mathbf{f}}}_m \in L_2 \bigcap L_\infty. \tag{36}$$

The proof directly follows (34) and (35). For the concept of *L_2 and L_∞ stability* (having similarities to *Lyapunov functions method*), see Appendix A.

IV. Slave Manipulator

A commercial HIAB-031 hydraulic manipulator is chosen to act as the slave manipulator of the teleoperation system. The manipulator is retrofitted with fast hydraulic servo valves, pressure transducers to measure cylinder chamber pressures, and high accuracy incremental encoders to measure joint angles. Although the manipulator is heavily retrofitted, it does not have force/torque sensor at the TCP. Consequently, a force-sensor-less control method with external force estimation is used for the slave manipulator as was the case with the master manipulator.

In the experiments, manipulation and force perception are considered within the same 2-DOF plane as with the master manipulator. The extension cylinder and rotation of the boom were mechanically locked. Fig. 4(a) illustrates the slave manipulator and shows several important frames of the manipulator. Frame $\{\mathbf{B_s}\}$ is fixed to the base of the slave manipulator, frame $\{\mathbf{O}_2\}$ is attached to the last link of the slave manipulator, and frame $\{\mathbf{G}\}$ is attached to the tip of the slave manipulator and has the same orientation as frame $\{\mathbf{O}_2\}$. Frame $\{\mathbf{C}\}$ has the same origin as frame $\{\mathbf{G}\}$, but is aligned with frame $\{\mathbf{B}_s\}$.

As discussed in Section I-B, *VDC enables modularity in the control design*. Consequently, the slave manipulator can be considered as a subsystem (with its own local subsystems) of the overall system. Stability-guaranteed constrained motion control of the slave manipulator has been demonstrated in [6]. Thus, taking advantage of the modular control design, only the control equations of the environment interacting object (see Object 2 in Figs. 4 and 5) need to be redesigned, while *rest*

This article has been accepted for inclusion in a future issue of this journal. Content is final as presented, with the exception of pagination.

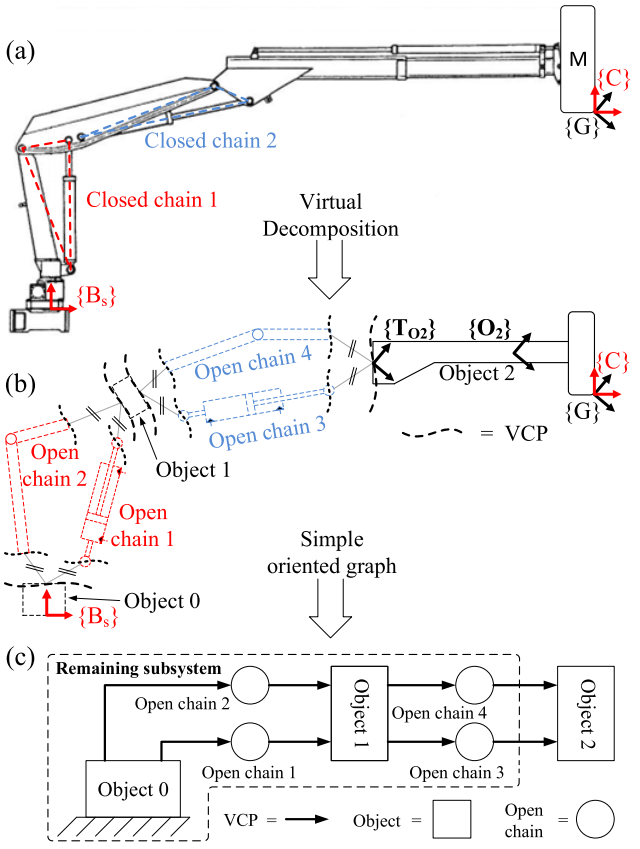

Fig. 4. (a) Slave manipulator. (b) Virtual decomposition of the slave manipulator. (c) Simple oriented graph (SOG) of the slave manipulator. The circled area in the SOG represents subsystem of the slave manipulator, for which the control has been designed in [6].

of the control system is kept identical to that of [6]. Fig. 4 presents the decomposed structure of the slave manipulator, with the reused control design circled by a dashed line.

A. Object 2—Kinematics and Dynamics

Let the linear/angular velocity vector ${}^{\mathbf{T}_{O2}}V \in \mathbb{R}^6$ at the driven VCP of Object 2 be known from the kinematic chain through the previous subsystems (see [6]). Then, kinematic transformations among the frames in Object 2 (see Fig. 5) can be written as

$$\begin{aligned} {}^{\mathbf{G}}V &= {}^{\mathbf{T}_{O2}}\mathbf{U}_{\mathbf{G}}^{T\,\mathbf{T}_{O2}}V \\ &= {}^{\mathbf{O}_2}\mathbf{U}_{\mathbf{G}}^{T\,\mathbf{O}_2}V \end{aligned} \tag{37}$$

$${}^{\mathbf{C}}V = \mathrm{diag}({}^{\mathbf{G}}\mathbf{R}_{\mathbf{C}}, {}^{\mathbf{G}}\mathbf{R}_{\mathbf{C}})^{\mathbf{G}}V. \tag{38}$$

Next, dynamics of the environment are defined. In this work, we assume flexible environment with dynamics described by second-order linear time-invariant model [22] as

$$\mathbf{f}_s = \mathbf{M}_e\ddot{\mathbf{x}}_s + \mathbf{D}_e\dot{\mathbf{x}}_s + \mathbf{K}_e\mathbf{x}_s \tag{39}$$

where $\mathbf{M}_e \in \mathbb{R}^{2\times2}$, $\mathbf{D}_e \in \mathbb{R}^{2\times2}$, and $\mathbf{K}_e \in \mathbb{R}^{2\times2}$ are symmetric positive-definite matrices approximating the inertia, damping, and stiffness of the environment, respectively, and $\mathbf{x}_s \in \mathbb{R}^2$ denotes the tip position of the slave manipulator, expressed in frame $\{\mathbf{B_s}\}$, subject to $\dot{\mathbf{x}}_s = \mathcal{V}_s$ with

$$\mathcal{V}_s = [\mathbf{I}_{2\times2} \quad \mathbf{0}_{2\times4}]{}^{\mathbf{C}}V. \tag{40}$$

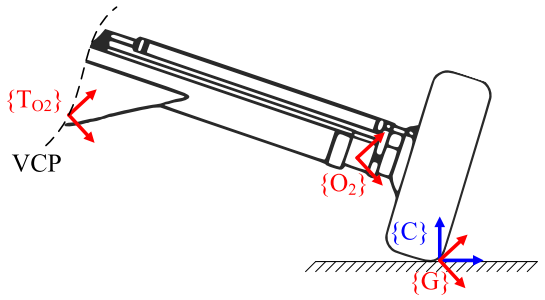

Fig. 5. Object 2 and its contact point with the environment.

Then, dynamics of the environment can be included on the slave manipulator as

$${}^{\mathbf{G}}F = \mathrm{diag}({}^{\mathbf{G}}\mathbf{R}_{\mathbf{C}}, {}^{\mathbf{G}}\mathbf{R}_{\mathbf{C}})[\mathbf{I}_{2\times2} \quad \mathbf{0}_{2\times4}]^T\sigma_f\mathbf{f}_s \tag{41}$$

where

$$\sigma_f = \begin{cases} 0, & \text{approach motion} \\ 1, & \text{constrained motion.} \end{cases}$$

The net force/moment vector (rigid body dynamics) ${}^{\mathbf{O}_2}F^*$ of Object 2 can be written in view of (3) as

$$\mathbf{M}_{\mathbf{O}_2}\frac{d}{dt}({}^{\mathbf{O}_2}V) + \mathbf{C}_{\mathbf{O}_2}({}^{\mathbf{O}_2}\omega){}^{\mathbf{O}_2}V + \mathbf{G}_{\mathbf{O}_2} = {}^{\mathbf{O}_2}F^* \tag{42}$$

and, eventually, the force balance (i.e. force resultant) equation of Object 2 can be written as

$${}^{\mathbf{O}_2}F^* = {}^{\mathbf{O}_2}\mathbf{U}_{\mathbf{T}_{O2}}{}^{\mathbf{T}_{O2}}F - \sigma_f{}^{\mathbf{O}_2}\mathbf{U}_{\mathbf{G}}{}^{\mathbf{G}}F. \tag{43}$$

Remark 4: Disturbances in (14) and (39) are neglected in this manuscript, but they may affect the performance in practical applications. Approximation of operator dynamics and environmental parameters can be applied to mitigate this problem. Such an approach is proposed in [19], where a fuzzy logic system is deployed to approximate these parameters.

B. Object 2—Control

Let the required velocity of the slave manipulator be designed as

$$\mathcal{V}_{sr} = \mathcal{V}_{sd} - \mathbf{A}\tilde{\hat{\mathbf{f}}}_s \tag{44}$$

where $\mathcal{V}_{sd} \in \mathbb{R}^2$ is to be defined in Section V, and $\tilde{\hat{\mathbf{f}}}_s \in \mathbb{R}^2$ is obtained from $\hat{\mathbf{f}}_s \in \mathbb{R}^2$ using a first-order filter as

$$\dot{\tilde{\hat{\mathbf{f}}}}_s + \mathbf{C}\tilde{\hat{\mathbf{f}}}_s = \mathbf{C}\hat{\mathbf{f}}_s \tag{45}$$

and $\hat{\mathbf{f}}_s$ is obtained using (15) in [6].

Required piston velocities of the slave manipulator are then redesigned from (87) in [6] into

$$\begin{bmatrix} \dot{x}_{1\mathrm{r}} \\ \dot{x}_{3\mathrm{r}} \end{bmatrix} = \mathbf{J}_x^{-1}\mathcal{V}_{sr} \tag{46}$$

where $\mathbf{J}_x^{-1} \in \mathbb{R}^{2\times2}$ is the invertible Jacobian matrix of the slave manipulator, defined in [6].

This article has been accepted for inclusion in a future issue of this journal. Content is final as presented, with the exception of pagination.

Then, in view of (37), (38), and (40), the required linear/angular velocity vectors in Object 2 can be written as

$$\begin{aligned} {}^{\mathbf{G}}V_r &= {}^{\mathbf{T}_{\mathrm{O2}}}\mathbf{U}_{\mathbf{G}}^{T}\,{}^{\mathbf{T}_{\mathrm{O2}}}V_r \\ &= {}^{\mathbf{O}_2}\mathbf{U}_{\mathbf{G}}^{T}\,{}^{\mathbf{O}_2}V_r \qquad (47) \\ {}^{\mathbf{C}}V_r &= \mathrm{diag}({}^{\mathbf{G}}\mathbf{R}_{\mathbf{C}}, {}^{\mathbf{G}}\mathbf{R}_{\mathbf{C}})\,{}^{\mathbf{G}}V_r \qquad (48) \\ \mathcal{V}_{sr} &= [\mathbf{I}_{2\times 2} \quad \mathbf{0}_{2\times 4}]\,{}^{\mathbf{C}}V_r. \qquad (49) \end{aligned}$$

The required contact force of the slave manipulator is designed as

$$\mathbf{f}_{sr} = \mathbf{M}_e\dot{\mathcal{V}}_{sr} + \mathbf{D}_e\dot{\mathbf{x}}_s + \mathbf{K}_e\mathbf{x}_s. \qquad (50)$$

Finally, using (22) and (41)–(43), the required control laws for Object 2 dynamics can be written as

$$\begin{aligned} {}^{\mathbf{G}}F_r &= \mathrm{diag}({}^{\mathbf{G}}\mathbf{R}_{\mathbf{C}}, {}^{\mathbf{G}}\mathbf{R}_{\mathbf{C}})[\mathbf{I}_{2\times 2} \quad \mathbf{0}_{2\times 4}]^T\sigma_f\mathbf{f}_{sr} \qquad (51) \\ {}^{\mathbf{O}_2}F_r^* &= \mathbf{Y}_{\mathbf{O}_2}\widehat{\boldsymbol{\theta}}_{\mathbf{O}_2} + \mathbf{K}_{\mathbf{O}_2}({}^{\mathbf{O}_2}V_{\mathrm{r}} - {}^{\mathbf{O}_2}V) \qquad (52) \\ {}^{\mathbf{O}_2}F_r^* &= {}^{\mathbf{O}_2}\mathbf{U}_{\mathbf{T}_{\mathrm{o2}}}\,{}^{\mathbf{T}_{\mathrm{o2}}}F_r - \sigma_f\,{}^{\mathbf{O}_2}\mathbf{U}_{\mathbf{G}}\,{}^{\mathbf{G}}F_r. \qquad (53) \end{aligned}$$

In line with (22), $\mathbf{Y}_{\mathbf{O}_2}\widehat{\boldsymbol{\theta}} \in \mathbb{R}^6$ in (52) is the model-based feedforward compensation term for the rigid body dynamics and $\mathbf{K}_{\mathbf{O}_2} \in \mathbb{R}^{6\times 6}$ is a positive-definite velocity feedback matrix to ensure the control stability. By defining

$$\mathbf{s}_{\mathbf{O}_2} = \mathbf{Y}_{\mathbf{O}_2}^T({}^{\mathbf{O}_2}V_{\mathrm{r}} - {}^{\mathbf{O}_2}V) \qquad (54)$$

the estimated parameter vector $\widehat{\boldsymbol{\theta}}_{\mathbf{O}_2} \in \mathbb{R}^{13}$ in (52) is updated as

$$\begin{aligned} \dot{\widehat{\theta}}_{\mathbf{O}_2 i} &= \rho_i s_{\mathbf{O}_2 i}\kappa_i \quad \forall i \in \{1, 2, \ldots, 13\} \\ \kappa_i &= \begin{cases} 0, & \widehat{\theta}_{\mathbf{O}_2 i} \le \theta^{-}_{\mathbf{O}_2 i} \text{ and } s_{\mathbf{O}_2 i} \le 0 \\ 0, & \widehat{\theta}_{\mathbf{O}_2 i} \ge \theta^{+}_{\mathbf{O}_2 i} \text{ and } s_{\mathbf{O}_2 i} \ge 0 \\ 1, & \text{otherwise} \end{cases} \qquad (55) \end{aligned}$$

where $\widehat{\theta}_{\mathbf{O}_2 i}$ is the ith element of $\widehat{\boldsymbol{\theta}}_{\mathbf{O}_2}$, $s_{\mathbf{O}_2 i}$ is the ith element of $\mathbf{s}_{\mathbf{O}_2}$, $\rho_i > 0$ is the update gain, $\theta^{-}_{\mathbf{O}_2 i}$ is the lower bound of $\widehat{\theta}_{\mathbf{O}_2 i}$, and $\theta^{+}_{\mathbf{O}_2 i}$ is the upper bound of $\widehat{\theta}_{\mathbf{O}_2 i}$.

C. Stability

The remaining system, for which the control was designed first in [6], qualifies as virtually stable according to Theorem 2.

Theorem 2: Consider the system encircled by a dashed line in Fig. 4. The subsystem qualifies virtually stable with its affiliated vector $({}^{\mathbf{A}}V_r - {}^{\mathbf{A}}V), \forall \mathbf{A} \in \Psi_r$ and its affiliated scalar variables $(f_{\mathrm{pi}r} - f_{\mathrm{p}i})$ for the hydraulic cylinder i, $\forall i \in 1, 2$, where Ψ_r contains the rigid body frames of each rigid link and object of the remaining subsystem. A non-negative accompanying function for this system can be found as

$$\begin{aligned} \nu_{\mathbf{R}} \ge \frac{1}{2}\sum_{A\in\Psi_{\mathrm{r}}}({}^{\mathbf{A}}V_{\mathrm{r}} - {}^{\mathbf{A}}V)^T\mathbf{M}_{\mathbf{A}}({}^{\mathbf{A}}V_{\mathrm{r}} - {}^{\mathbf{A}}V) \\ + \frac{1}{2}\sum_{i=1}^{2}\left[\frac{1}{\beta k_{\mathrm{xi}}}(f_{\mathrm{pi}r} - f_{\mathrm{p}i})^2\right] \qquad (56) \end{aligned}$$

such that

$$\begin{aligned} \dot{\nu}_{\mathbf{R}} \leqslant -\sum_{A\in\Psi_{\mathrm{r}}}({}^{\mathbf{A}}V_{\mathrm{r}} - {}^{\mathbf{A}}V)^T\mathbf{K}_{\mathbf{A}}({}^{\mathbf{A}}V_{\mathrm{r}} - {}^{\mathbf{A}}V) - p_{\mathbf{T}_{\mathrm{O2}}} \\ - \frac{k_f}{k_x}\sum_{i=1}^{2}(f_{\mathrm{pi}r} - f_{\mathrm{p}i}). \qquad (57) \end{aligned}$$

Proof: The proof for Theorem 2 can be obtained from the results of [6]. □

Theorem 3: Consider Object 2 described by (37)–(43), combined with the control equations (44)–(53) and with the parameter adaptation (54)–(55). This subsystem is virtually stable with its affiliated vector ${}^{\mathbf{O}_2}V_r - {}^{\mathbf{O}_2}V$ being a virtual function in both L_2 and L_∞ in the sense of Definition 3. This is because a non-negative accompanying function

$$\begin{aligned} \nu_{\mathbf{O}_2} = \frac{1}{2}({}^{\mathbf{O}_2}V_{\mathrm{r}} - {}^{\mathbf{O}_2}V)^T\mathbf{M}_{\mathbf{O}_2}({}^{\mathbf{O}_2}V_{\mathrm{r}} - {}^{\mathbf{O}_2}V) \\ + \frac{1}{2}\sum_{i=1}^{13}\frac{(\theta_{\mathbf{O}_2 i} - \widehat{\theta}_{\mathbf{O}_2 i})^2}{\rho_{\mathbf{O}_2 i}} \qquad (58) \end{aligned}$$

can be found such that

$$\dot{\nu}_{\mathbf{O}_2} \leqslant -({}^{\mathbf{O}_2}V_{\mathrm{r}} - {}^{\mathbf{O}_2}V)^T\mathbf{K}_{\mathbf{O}_2}({}^{\mathbf{O}_2}V_{\mathrm{r}} - {}^{\mathbf{O}_2}V) + p_{\mathbf{T}_{\mathrm{O2}}} - p_{\mathbf{G}} \qquad (59)$$

holds, where

$$\int_0^\infty p_{\mathbf{G}}(t)dt \geqslant -\gamma_s \qquad (60)$$

holds with $0 \leqslant \gamma_s < \infty$. Note that $p_{\mathbf{T}_{\mathrm{O2}}}$ is the VPF by Definition 2 in the driven VCP of Object 2, and $p_{\mathbf{G}}$ characterizes the VPF between the end-effector and the environment while in constrained motion (i.e., $\sigma_f = 1$).

Proof: See Appendix C. □

Theorem 4: Considering (87) and Definition 3, the contact with the environment qualifies virtually stable. The non-negative accompanying function for the entire slave manipulator can be obtained by summing the individual functions from (56) and (58).

Stability analysis for the remaining subsystems follows exactly as shown in [6], ultimately yielding stability of the entire slave robot, as it follows:

$$\xi_s \equiv \mathcal{V}_{sd} - \mathcal{V}_s - \mathbf{A}\tilde{\tilde{\mathbf{f}}}_s \in L_2 \bigcap L_\infty. \qquad (61)$$

V. Teleoperation

After individual velocity-based controllers for both master and slave manipulators (see (25) and [6]) of the teleoperation system have been designed, a scheme for connecting the manipulators can be designed. Connection between the two manipulators is made with a *communication channel* that virtually connects the manipulators together. This section designs bilateral teleoperation and specifies two design vectors $\mathcal{V}_{md}$ and $\mathcal{V}_{sd}$, used in (18) and (44), respectively. Using position control $\delta = 1$ in [22], $\mathcal{V}_{md}$ and $\mathcal{V}_{sd}$ can be designed as

$$\begin{aligned} \mathcal{V}_{md} = \frac{1}{\kappa_p}[\tilde{\mathcal{V}}_s + \Lambda(\tilde{\mathcal{P}}_s - \kappa_p\mathcal{P}_m) \\ - \mathbf{A}(\tilde{\tilde{\mathbf{f}}}_s + (\kappa_f - \kappa_p)\tilde{\tilde{\mathbf{f}}}_m)] \qquad (62) \\ \mathcal{V}_{sd} = \kappa_p\tilde{\mathcal{V}}_m - \Lambda(\mathcal{P}_s - \kappa_p\tilde{\mathcal{P}}_m) - \mathbf{A}\kappa_f\tilde{\tilde{\mathbf{f}}}_m \qquad (63) \end{aligned}$$

where $\kappa_p > 0$ and $\kappa_f > 0$ are position and force scaling factors *for arbitrary motion/force scaling between the manipulators*, $\Lambda \in \mathbb{R}^{2\times 2}$ is a diagonal positive-definite matrix, and $\mathcal{P}_m \in \mathbb{R}^2$ and $\mathcal{P}_s \in \mathbb{R}^2$ denote the position/orientation of the master and slave manipulator, respectively, subject to $\dot{\mathcal{P}}_m = \mathcal{V}_m$ and

This article has been accepted for inclusion in a future issue of this journal. Content is final as presented, with the exception of pagination.

$\dot{\mathcal{P}}_s = \mathcal{V}_s$. Furthermore, $\tilde{\mathcal{V}}_m$, $\tilde{\mathcal{V}}_s$, $\tilde{\mathcal{P}}_m$, and $\tilde{\mathcal{P}}_s$ are filtered values of $\mathcal{V}_m$, $\mathcal{V}_s$, $\mathcal{P}_m$, and $\mathcal{P}_s$, respectively, obtained using the following first-order filter:

$$\dot{\tilde{\mathcal{X}}} + \mathbf{C}\tilde{\mathcal{X}} = \mathbf{C}\mathcal{X} \tag{64}$$

where $\mathcal{X} \in \mathbb{R}^2$ is the input signal and $\tilde{\mathcal{X}} \in \mathbb{R}^2$ is the filtered signal. The use of filtered variables in the two design vectors, (63) and (62), makes the required accelerations $\dot{\mathcal{V}}_{sd}$ and $\dot{\mathcal{V}}_{md}$ functions of $\mathcal{V}_m$, $\mathcal{V}_s$, $\mathbf{f}_m$, and $\mathbf{f}_s$.

A. Tracking

Substituting (62) and (63) into (36) and (61) and then subtracting the resulting error terms from each other yields

$$\kappa_p\xi_m - \xi_s = (\mathcal{V}_s - \kappa_p\mathcal{V}_m) + \Lambda(\mathcal{P}_s - \kappa_p\mathcal{P}_m) + (\tilde{\mathcal{V}}_s - \kappa_p\tilde{\mathcal{V}}_m) + \Lambda(\tilde{\mathcal{P}}_s - \kappa_p\tilde{\mathcal{P}}_m). \tag{65}$$

It can be easily seen that (65) can be further written as

$$\kappa_p\xi_m - \xi_s = \tilde{\mathcal{Z}} + \mathcal{Z} \tag{66}$$

where

$$\mathcal{Z} \equiv (\mathcal{V}_s - \kappa_p\mathcal{V}_m) + \Lambda(\mathcal{P}_s - \kappa_p\mathcal{P}_m) \tag{67}$$

and $\tilde{\mathcal{Z}}$ is obtained from $\mathcal{Z}$ using (64).

Following Lemma 2.4 in [22] yields

$$\mathcal{Z} \in L_2 \bigcap L_\infty. \tag{68}$$

Eventually, it follows from (67), (68) and Lemma 1 in [22] that

$$\xi_v = \kappa_p\mathcal{V}_m - \mathcal{V}_s \in L_2 \bigcap L_\infty \tag{69}$$

$$\xi_p = \kappa_p\mathcal{P}_m - \mathcal{P}_s \in L_2 \bigcap L_\infty \tag{70}$$

hold, which guarantees the L_2 and L_∞ stability of the velocity and position tracking of the teleoperation system.

B. Transparency

Transparency of the teleoperation system can be analyzed by substituting (62) and (63) into (36) and (61), then summing the resulting error terms together results in

$$\kappa_p\xi_m + \xi_s(\tilde{\mathcal{V}}_s - \mathcal{V}_s) + \kappa_p(\tilde{\mathcal{V}}_m - \mathcal{V}_m) + \Lambda(\tilde{\mathcal{P}}_s - \mathcal{P}_s) + \Lambda\kappa_p(\tilde{\mathcal{P}}_m - \mathcal{P}_m) - 2\mathbf{A}(\tilde{\hat{\mathbf{f}}}_s + \kappa_f\tilde{\mathbf{f}}_m). \tag{71}$$

Substituting (64) with $-\mathbf{C}^{-1}\dot{\tilde{\mathcal{X}}} = (\tilde{\mathcal{X}} - \mathcal{X})$ into (71) yields

$$\kappa_p\xi_m + \xi_s = -\mathbf{C}^{-1}[\dot{\tilde{\mathcal{V}}}_s + \kappa_p\dot{\tilde{\mathcal{V}}}_m + \Lambda\tilde{\mathcal{V}}_s + \Lambda\kappa_p\tilde{\mathcal{V}}_m] - 2\mathbf{A}(\tilde{\hat{\mathbf{f}}}_s + \kappa_f\tilde{\mathbf{f}}_m). \tag{72}$$

According to [22], we can rewrite (72), using (69)–(70), as

$$-\tilde{\mathbf{f}}_m = \kappa_f^{-1}\tilde{\mathbf{f}}_s + \kappa_f^{-1}\kappa_p\mathbf{A}^{-1}\mathbf{C}^{-1}(s+\Lambda)\tilde{\mathcal{V}}_m + \frac{\xi}{2\kappa_f} \tag{73}$$

where s denotes the Laplace operator, and

$$\xi \equiv \mathbf{A}^{-1}[-\mathbf{C}^{-1}(s+\Lambda)\tilde{\xi}_v + (\xi_s + \kappa_p\xi_m)] \tag{74}$$

where $\tilde{\xi}_v$ is obtained from ξ_v using (64). In view of Lemma 1 in [22], the following holds true:

$$\xi \in L_2 \bigcap L_\infty.$$

Transparency of the teleoperation system can be seen from (73). Within a limited frequency range, the filtered signals can be assumed to be approximately equal to their nonfiltered counterparts. The last term on the right-hand side of (73) is bounded to converge to zero. Then, the transparency error can be described by the second term on the right-hand side of (73). It comprises of velocity- and acceleration-dependent terms. The acceleration-related term $\kappa_f^{-1}\kappa_p\mathbf{A}^{-1}\mathbf{C}^{-1}$ acts as a *virtual mass* on the teleoperation system, while the velocity-dependent term $\kappa_f^{-1}\kappa_p\mathbf{A}^{-1}\mathbf{C}^{-1}\Lambda$ determines the *damping* of the teleoperation system.

C. Stability Under Time Delay

Time delay under teleoperation is a much investigated issue especially in space teleoperation. Although the focus of this study is in terrestrial applications, robustness against arbitrary time delay of the proposed method is discussed briefly. In [13], similar approach was used for longer and varying delays.

Without loss of generality, we consider a 1-D system in the stability analysis. The extension to multiple-dimensional systems can be proceeded accordingly. Due to the fact that both master and slave manipulators have independent stability-guaranteed controllers linked only by the communication channel, the stability under time delay can be analyzed by modifying (62) and (63) as

$$\mathcal{V}_{md} = \kappa_p^{-1}[e^{-sT}(\tilde{\mathcal{V}}_s + \Lambda\tilde{\mathcal{P}}_s) - \kappa_p\Lambda\mathcal{P}_m - \mathbf{A}(e^{-sT}\tilde{\hat{\mathbf{f}}}_s + (\kappa_f - \kappa_p)\tilde{\hat{\mathbf{f}}}_m)] \tag{75}$$

$$\mathcal{V}_{sd} = e^{-sT}\kappa_p(\tilde{\mathcal{V}}_m - \Lambda\tilde{\mathcal{P}}_m) - \Lambda\mathcal{P}_s - e^{-sT}\mathbf{A}\kappa_f\tilde{\hat{\mathbf{f}}}_m \tag{76}$$

where the communication channel is represented as pure time delay of T (see Fig. 6). The stability under arbitrary time delay can be analyzed similar to the method presented in [22].

Fig. 6 represents the teleoperation system under arbitrary time delay based on (75) and (76). In the figure, Z_h is the operator dynamics defined in (14) (now considered 1-D) and Z_e is environment dynamics, which is approximated with second-order linear dynamics. Sufficient condition for stability under time delay can then be summarized as

$$\mathbf{b} + 4C\sqrt{\Lambda AK(2ACM+1)} \geq 0 \tag{77}$$

where

$$\mathbf{b} = \Lambda^2 + 2AC(2ACD - K - 2\Lambda ACM).$$

The detailed steps leading to (77) are shown in Appendix D.

VI. Experiments

This section evaluates the performance of the proposed teleoperation system. First, Section VI-A addresses the system implementation issues. Then, Section VI-B provides the experiments without time delay, followed by the experiment with time delay in Section VI-C.

This article has been accepted for inclusion in a future issue of this journal. Content is final as presented, with the exception of pagination.

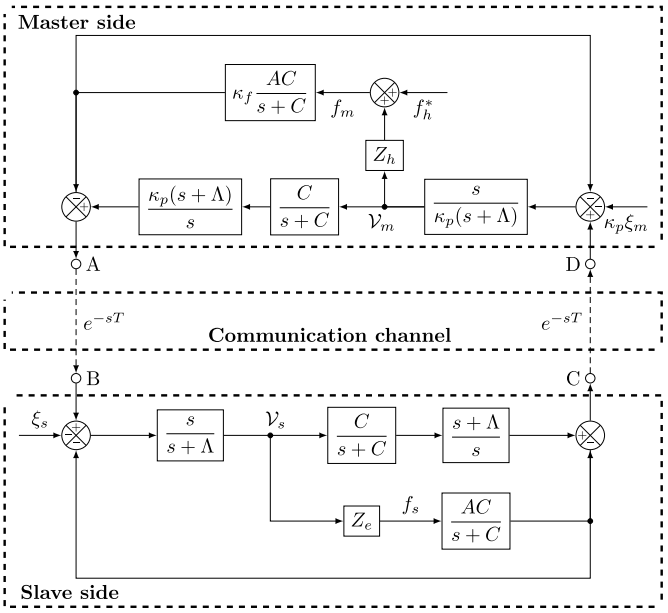

Fig. 6. 1-D block diagram representation of the teleoperation system under arbitrary time delay of T.

TABLE I
USED COMMUNICATION CHANNEL PARAMETERS

	κ_p	κ_f	Λ	**A**	**C**
Experiment 1:	1	300	2.0	60×10^{-6}	35
Experiment 2:	4	800	2.0	100×10^{-6}	35
Experiment 3:	1.5	500	1.5	40×10^{-6}	35

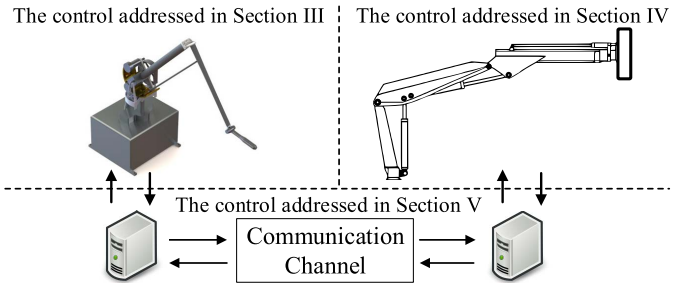

Fig. 7. High-level overview of the experimental implementation.

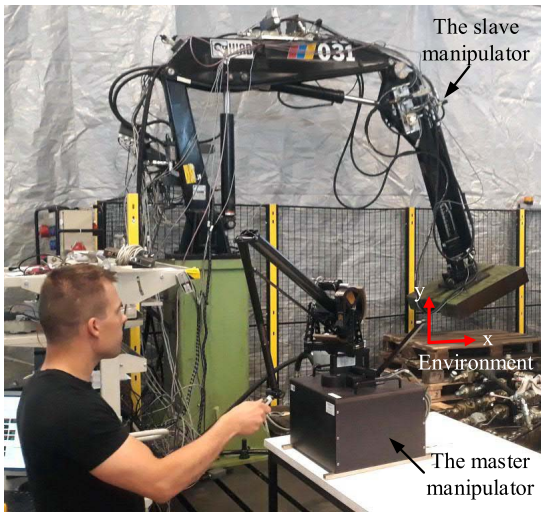

Fig. 8. Experimental implementation and setup.

A. Experiment Description

The experimental implementation comprises four main components, visualized in Fig. 7, which are the electric master manipulator (Phantom Premium 6DOF/3.0L haptic device), the host computer for the master manipulator, the real-time computer, and the hydraulic slave manipulator (HIAB-031 manipulator). The 2-DOF hydraulic manipulator (in Fig. 8) has a maximum reach of approximately 3.2 m, and a payload of 475 kg is attached to its tip. For the real-time control system, the following components were used: a DS1005 processor board, a DS3001 incremental encoder board, a DS2103 DAC board, a DS2003 ADC board, and a DS4504 100 Mb/s Ethernet interface. The remaining hardware implementations can be found in [6], [11] or [23]. Control computations have been run with 500-Hz frequency. The communication channel parameters of each experiment are shown in Table I.

Teleoperation control between the master and slave manipulators was engaged by pressing a pushbutton and disengaged by releasing the button. At first, the slave manipulator was driven from free space to contact with the environment along the Cartesian y-axis (see Fig. 8 for the directions of the Cartesian coordinate system). After contact with the environment was established, the slave manipulator was driven along the surface of the pallets, while maintaining constant force against the environment. Finally, the slave manipulator was driven back to free space after approximately 0.5 m of sliding against the wooden pallets. The above described task was repeated *without any time delay* with two different sets of motion/force scaling parameters (κ_p and κ_f) of the communication system (see Fig. 9). Then, an experiment *with 80-ms one-way time delay* in the communication channel was performed (see Fig. 10). In Figs. 9 and 10, the master manipulator data is shown in blue, and the slave manipulator data in red.

B. Experiments Without Time Delay

In the *first experiment* [Fig. 9(a)], 1:1 position mapping was used between the manipulators ($\kappa_p = 1$), while forces of the master manipulator were scaled up by a factor of $\kappa_f = 300$ (see Table I). In the *second experiment* [Fig. 9(b)], 4:1 position scaling between the master and slave manipulators was used ($\kappa_p = 4$), yielding four times larger movement of the slave manipulator compared to the movement of the master manipulator, along with force scaling by a factor of $\kappa_f = 800$ (see Table I).

As Fig. 9 shows, accurate position (see the *first* and *second rows*) and force tracking (the *third* and *fourth rows*) between the master and slave manipulators is achieved with different scaling parameters, as predicted by the theory, despite the inherent challenges of force control of hydraulic manipulator in the teleoperation system (see the discussion in

This article has been accepted for inclusion in a future issue of this journal. Content is final as presented, with the exception of pagination.

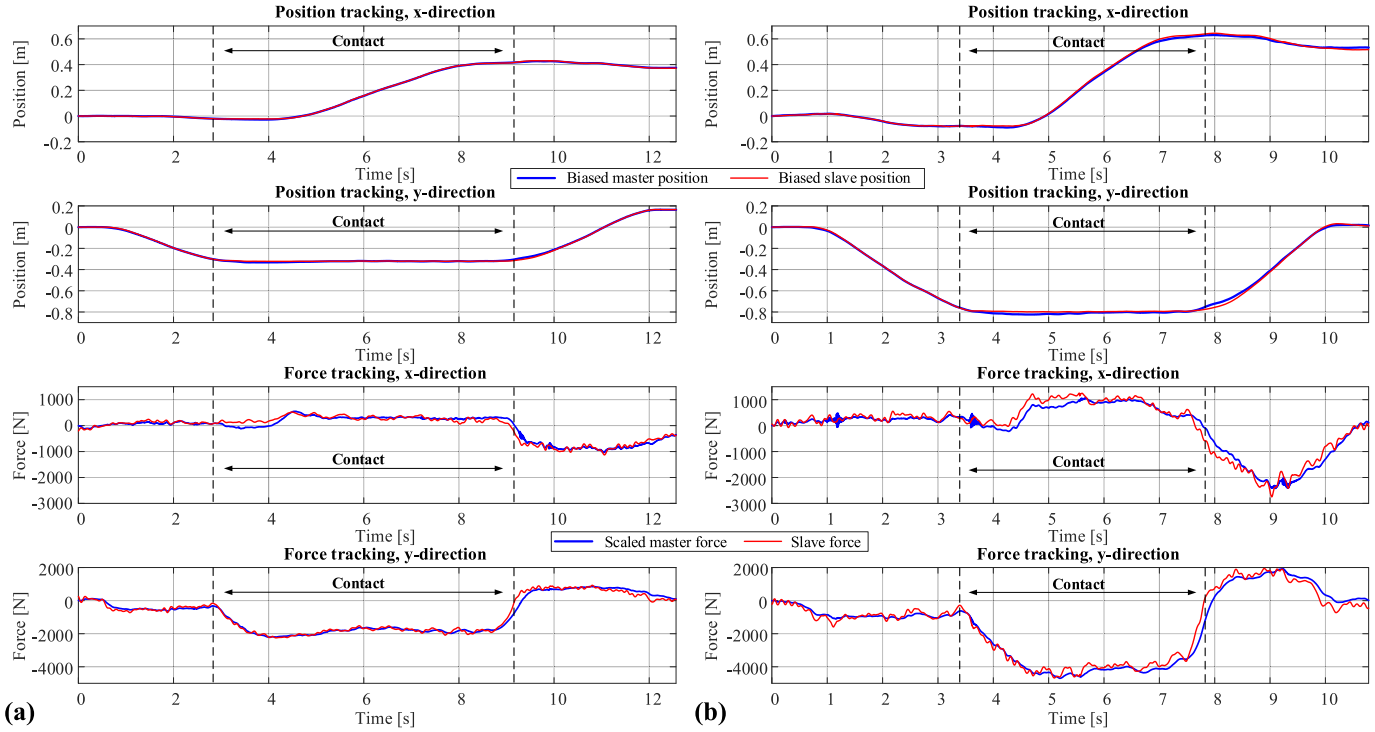

Fig. 9. Results from experimental implementation with bilateral force-reflected teleoperation. In the experiments, two different set of scaling parameters in the communication system were used as: (a) $\kappa_p = 1.0$ and $\kappa_f = 300$, and (b) $\kappa_p = 4.0$ and $\kappa_f = 800$. Scaling of the axes of the figures is kept the same between the two experiments to elaborate the effect of the scaling parameters to the behavior of the system.

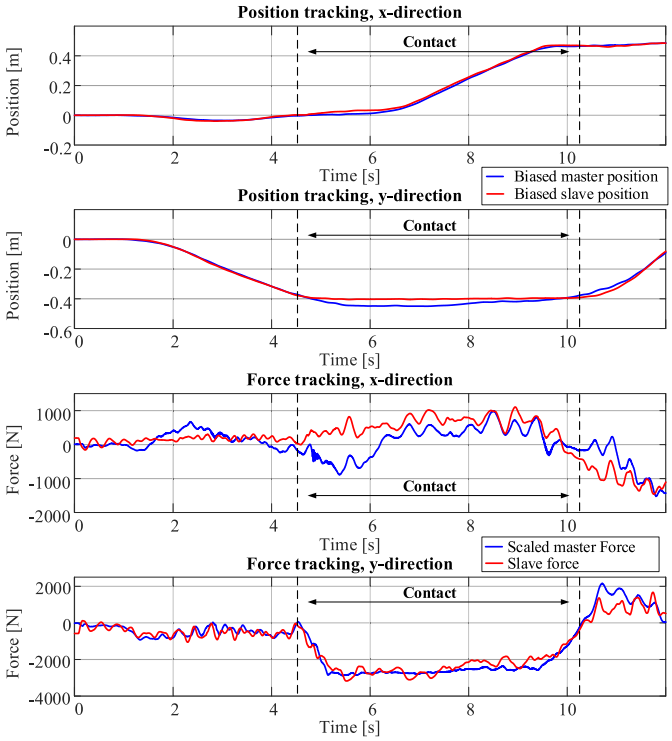

Fig. 10. Teleoperation task under one-way time delay of 80 ms. Parameters of the communication channel were set as: $\kappa_p = 1.5$ and $\kappa_f = 500$, $\Lambda = 1.5$, $\mathbf{C} = 35$, and $\mathbf{A} = 40 \times 10^{-6}$.

Section I). The forces in the third and fourth rows presents the *estimated* contact forces of the slave and master manipulators along the x- and y-axes, respectively. In the results, the master manipulator forces are scaled up by the respective scaling factor.

Table II shows the maximum and mean Cartesian tracking errors for each individual experiment. For objective motion tracking performance evaluation and to set a benchmark for future developments, a normalizing performance indicator $\rho = \max(\|\kappa_p X_m - X_s\|_2)/\max(\|\dot{X}_s\|_2)$ values are also reported in Table II (see [5] and [28] for more details on ρ). Comparative results from our preliminary study in [23] with the same system are also reported in Table II. The results from that study are mostly relevant compared to experiment 1 of this study due to similar scaling values. Improved motion and force tracking can be noticed as well as the improved performance indicator value.

Note that the slave manipulator contact forces are estimated from chamber pressures of the cylinder. Thus, some inaccuracies can exist in the measured contact forces (see [11] for more details). However, the operator is still able to effectively sense the contact forces between the slave and the environment, and excessive contact forces can be prevented. It is valid to mention that the proposed force sensorless approach provides a practical solution for teleoperation of extremely powerful hydraulic manipulators, as conventional 6-DOF force/torque sensors are fragile and prone to overloading [6].

Remark 5: Note that in the second experiment, the transition from free space motion to contact motion was done rapidly with a velocity of approximately 0.2 m/s. This is to demonstrate the stable behavior of the control system even with high velocity and rapid changes of system states.

C. Experiment With One-Way Time Delay of 80 ms

Fig. 10 shows respective results as in Fig. 9 with one-way time delay of 80 ms. To demonstrate the versatility, in the experiment, the scaling factors were selected as $\kappa_p = 1.5$

This article has been accepted for inclusion in a future issue of this journal. Content is final as presented, with the exception of pagination.

TABLE II
CARTESIAN TRACKING ERRORS DURING EXPERIMENTS

	Position error [mm] mean	max	Force error [N] mean	max	Perf. index ρ [s]
Experiment 1:	3.60	14.9	141	801	0.060
Experiment 2:	12.6	37.7	307	1476	0.074
Experiment 3:	19.4	50.4	467	1632	0.158
Exp. in [23]:	13.8	31.2	406	1111	0.147

and $\kappa_f = 500$. As the results indicate, the proposed method: 1) is robust against time delays and communication noises (as predicted by the theory in Section V-C) and 2) is capable of handling the delay without significant loss of performance.

VII. CONCLUSION

This study presented force-reflected bilateral teleoperation using asymmetric electrical master and hydraulic slave manipulators. The control design takes advantage of the VDC approach, which allows us to design local subsystem-dynamics-based controllers for the master and slave manipulators independently. Then, the teleoperation system was completed by designing the communication channel between the master and slave controllers as motivated by Zhu and Salcudean [22]. The teleoperation scheme provided unique features, such as arbitrary motion/force scaling between the manipulators, effectively enabling both micro- and macro-manipulations with appropriate force levels, which is an essential feature for asymmetric teleoperation systems.

The experimental results demonstrated the performance of the proposed method and showed excellent motion and force tracking between the manipulators. Furthermore, robustness against an arbitrary time delay was demonstrated theoretically and experimentally. Similar to our previous studies [6], [11], and [35], tracking performance improvements can be expected after rigorous application of a full parameter adaptation implementation and with tuning of the system parameters.

The aim of our research is to enable the use of LfD approaches on heavy-duty manipulators. Teleoperation is seen as a key enabling technology for the use of LfD-type methods safely on large-scale manipulators that cannot be taught by kinesthetic teaching. Our vision is that in the future, large manipulators can be taught to perform various tasks with the same ease as programming of lightweight arms. Alternatively, teleoperation can be used as such, as an intuitive and precise control method for large work machines. The proposed approach is demonstrated on commercially available hardware, and the fact that no force/torque sensor is required makes this approach very appealing for commercial use. Our interests lie in terrestrial low-latency force-reflecting teleoperation over the emerging cellular 5G networks. This article lays down experimentally verified control theoretic foundation, advancing force-reflected bilateral teleoperation control one more step toward practical applications in a wide variety of industrial applications of controlling heavy-duty machinery. The theoretical and experimental studies in this article concluded that the use of a force-sensor-less design for bilateral teleoperation is feasible.

Future work will focus on maximizing the system performances of position tracking and transparency, as well as forming basis functions for human operator exogenous forces through machine learning. Moreover, we intend to focus on expanding the experimental system to possess more DOFs with the goal of achieving a 6-DOF manipulation.

APPENDIX A
L_2 AND L_∞ STABILITY

Definition 1 provides a definition for the Lebesgue space.

Definition 1 [26]: The Lebesgue space, denoted as L_p with p being a positive integer, contains all Lebesgue measurable and integrable functions $f(t)$ subject to

$$\|f\|_p = \lim_{T\to\infty}\left[\int_0^T |f(t)|^p d\tau\right]^{\frac{1}{p}} < +\infty. \tag{78}$$

Two particular cases are considered:

1) A Lebesgue measurable function $f(t)$ belongs to L_2 if and only if $\lim_{T\to\infty}\int_0^T |f(t)|^2 d\tau < +\infty$.
2) A Lebesgue measurable function $f(t)$ belongs to L_∞ if and only if $\max_{t\in[0,\infty)}|f(t)| < +\infty$.

Lemma 1 (a simplified version of Lemma 2.3 in [26]) provides that a system is L_2 and L_∞ stable with its affiliated vector $\mathbf{x}(t)$, being a function in L_∞ and its affiliated vector $\mathbf{y}(t)$, being a function in L_2.

Lemma 1 [26]: Consider a non-negative differentiable function $\xi(t)$ defined as

$$\xi(t) \geqslant \frac{1}{2}\mathbf{x}(t)^T\mathbf{P}\mathbf{x}(t) \tag{79}$$

with $\mathbf{x}(t) \in \mathbb{R}^n$, $n \geqslant 1$, and $\mathbf{P} \in \mathbb{R}^{n\times n}$ being a symmetric positive-definite matrix. If the time-derivative of $\xi(t)$ is Lebesgue integrable and governed by

$$\dot{\xi}(t) \leqslant -\mathbf{y}(t)^T\mathbf{Q}\mathbf{y}(t) - s(t) \tag{80}$$

where $\mathbf{y}(t) \in \mathbb{R}^m$, $m \geqslant 1$, and $\mathbf{Q} \in \mathbb{R}^{m\times m}$ being a symmetric positive-definite matrix, and $s(t)$ is subject to

$$\int_0^\infty s(t)dt \geqslant -\gamma_0 \tag{81}$$

with $0 \leqslant \gamma_0 < \infty$, then, it follows that $\xi(t) \in L_\infty$, $\mathbf{x}(t) \in L_\infty$, and $\mathbf{y}(t) \in L_2$ hold.

Lemma 2 provides an alternative to Barbalat's lemma.

Lemma 2 [36]: If $e(t) \in L_2$ and $\dot{e}(t) \in L_\infty$, then $\lim_{t\to\infty} e(t) = 0$.

Remark 6: As a distinction to Lyapunov approaches, Lemma 1 allows different appearances of variables in the non-negative function itself and in its time-derivative. When all error signals are proved to belong to L_2 and L_∞ in the sense of Lemma 1, then asymptotic stability can be proved with Lemma 2, if the time-derivatives of all error signals belong to L_∞. Note that $s(t) = 0$ is a special case that satisfies (81) in Lemma 1.

This article has been accepted for inclusion in a future issue of this journal. Content is final as presented, with the exception of pagination.

APPENDIX B
VIRTUAL STABILITY

The unique feature of the VDC approach is the introduction of a scalar term, namely the VPF [26] (see Definition 2). The VPFs uniquely define the dynamic interactions among the subsystems and play an important role in the definition of *virtual stability* [26], which is defined in a simplified form in Definition 3.

Definition 2 [26]: The VPF with respect to frame $\{\mathbf{A}\}$ is the inner product of the linear/angular velocity vector error and the force/moment vector error as

$$p_{\mathbf{A}} = ({}^{\mathbf{A}}V_{\mathrm{r}} - {}^{\mathbf{A}}V)^T({}^{\mathbf{A}}F_{\mathrm{r}} - {}^{\mathbf{A}}F) \tag{82}$$

where ${}^{\mathbf{A}}V_{\mathrm{r}} \in \mathbb{R}^6$ and ${}^{\mathbf{A}}F_{\mathrm{r}} \in \mathbb{R}^6$ represent the required vectors of ${}^{\mathbf{A}}V \in \mathbb{R}^6$ and ${}^{\mathbf{A}}F \in \mathbb{R}^6$, respectively.

Definition 3 [26]: A subsystem with a *driven* VCP to which frame $\{\mathbf{A}\}$ is attached and a *driving* VCP to which frame $\{\mathbf{C}\}$ is attached is said to be virtually stable with its affiliated vector $\mathbf{x}(t)$ being a virtual function in L_∞ and its affiliated vector $\mathbf{y}(t)$ being a virtual function in L_2, if and only if there exists a non-negative accompanying function

$$v(t) \geqslant \frac{1}{2}\mathbf{x}(t)^T\mathbf{P}\mathbf{x}(t) \tag{83}$$

such that

$$\dot{v}(t) \leqslant -\mathbf{y}(t)^T\mathbf{Q}\mathbf{y}(t) - s(t) + p_{\mathbf{A}} - p_{\mathbf{C}} \tag{84}$$

holds,

$$\int_0^\infty s(t)d\tau \geqslant -\gamma_s \tag{85}$$

where $0 \leqslant \gamma_0 < \infty$, $\mathbf{P}$, and $\mathbf{Q}$ are two block-diagonal positive-definite matrices, and $p_{\mathbf{A}}$ and $p_{\mathbf{C}}$ denote the VPFs (by Definition 2) at frames $\{\mathbf{A}\}$ and $\{\mathbf{C}\}$, respectively.

Remark 7: In view of Theorem 2.1 in [26], when all subsystems qualify as *virtually stable* (in the sense of Definition 3), the L_2 and L_∞ stability of the entire system can be guaranteed in the sense Lemma 1.

APPENDIX C
PROOF OF THEOREM 3

According to Definition 2 and (39), (38), (41), (50), (48), and (51), it follows that

$$\begin{aligned}
p_{\mathbf{G}} &= ({}^{\mathbf{G}}V_{\mathrm{r}} - {}^{\mathbf{G}}V)^T({}^{\mathbf{G}}F_{\mathrm{r}} - {}^{\mathbf{G}}F) \\
&= ({}^{\mathbf{G}}V_{\mathrm{r}} - {}^{\mathbf{G}}V)^T\mathrm{diag}({}^{\mathbf{G}}\mathbf{R}_{\mathbf{C}}, {}^{\mathbf{G}}\mathbf{R}_{\mathbf{C}}) \\
&\quad \times [\mathbf{I}_{2\times 2} \quad \mathbf{0}_{2\times 4}]^T\sigma_f(\mathbf{f}_{sr} - \mathbf{f}_s) \\
&= ({}^{\mathbf{G}}V_{\mathrm{r}} - {}^{\mathbf{G}}V)^T\mathrm{diag}({}^{\mathbf{G}}\mathbf{R}_{\mathbf{C}}, {}^{\mathbf{G}}\mathbf{R}_{\mathbf{C}}) \\
&\quad \times [\mathbf{I}_{2\times 2} \quad \mathbf{0}_{2\times 4}]^T\sigma_f\mathbf{M}_e(\dot{\mathcal{V}}_{sr} - \dot{\mathcal{V}}_s) \\
&= \left({}^{\mathbf{C}}V_{\mathrm{r}} - {}^{\mathbf{C}}V\right)^T[\mathbf{I}_{2\times 2} \quad \mathbf{0}_{2\times 4}]^T\sigma_f\mathbf{M}_e(\dot{\mathcal{V}}_{sr} - \dot{\mathcal{V}}_s) \\
&= \sigma_f(\mathcal{V}_{sr} - \mathcal{V}_s)^T\mathbf{M}_e(\dot{\mathcal{V}}_{sr} - \dot{\mathcal{V}}_s).
\end{aligned} \tag{86}$$

For a constant value of σ_f, the following holds true:

$$\begin{aligned}
\int_0^\infty p_{\mathbf{G}}dt &= \int_0^\infty \sigma_f(\mathcal{V}_{sr} - \mathcal{V}_s)^T\mathbf{M}_e(\dot{\mathcal{V}}_{sr} - \dot{\mathcal{V}}_s)dt \\
&\geq -\frac{1}{2}\sigma_f(\mathcal{V}_{sr}(0) - \mathcal{V}_s(0))^T\mathbf{M}_e(\mathcal{V}_{sr}(0) - \mathcal{V}_s(0))
\end{aligned} \tag{87}$$

APPENDIX D
STABILITY UNDER TIME DELAY

To analyze the effect of time delay on the system stability, transfer functions on both sides of the communication channel need to be defined. The transfer function for the master side, from input D to output A (see Fig. 6), can be formed as

$$\begin{aligned}
G_m &= \frac{\frac{C}{s+C} - \frac{sAC\frac{\kappa_f}{\kappa_p}Z_h}{(s+\Lambda)(s+C)}}{1 + \frac{sAC\frac{\kappa_f}{\kappa_p}Z_h}{(s+\Lambda)(s+C)}} \\
&= \frac{-ACM_h^*s^2 + \left(C - ACD_h^*\right)s + \left(C\Lambda - ACK_h^*\right)}{\left(1+ACM_h^*\right)s^2 + \left(\Lambda + C + ACD_h^*\right)s + \left(\Lambda C + ACK_h^*\right)}
\end{aligned} \tag{88}$$

where $M_h^* = (\kappa_f/\kappa_p)M_h$, $D_h^* = (\kappa_f/\kappa_p)D_h$, and $K_h^* = (\kappa_f/\kappa_p)K_h$.

Following the same procedure, the transfer function from the input B of the slave side to output C can be formed as

$$G_s = \frac{\frac{C}{s+C} - \frac{sACZ_e}{(s+\Lambda)(s+C)}}{1 + \frac{sACZ_e}{(s+\Lambda)(s+C)}}. \tag{89}$$

Assume flexible environment with dynamics as

$$Z_e = M_es + D_e + \frac{K_e}{s} \tag{90}$$

where M_e, D_e, and K_e define the inertia, damping, and stiffness of the environment, respectively.

Then, the transfer function from B to C can be written as

$$G_s = \frac{-ACM_es^2 + (C - ACD_e)s + (C\Lambda - ACK_e)}{(1 + ACM_e)s^2 + (\Lambda + C + ACD_e)s + (\Lambda C + ACK_e)}. \tag{91}$$

To guarantee stability under arbitrary time delay, the gain of each manipulator together with their respective local controllers must remain equal to or smaller than the one across the entire frequency spectrum. Thus, to ensure stability of the entire teleoperation system with arbitrary time delay (see Fig. 6), the following conditions need to be satisfied:

$$\left\| \frac{-ACM_h^*(j\omega)^2 + \left(C - ACD_h^*\right)(j\omega) + \left(C\Lambda - ACK_h^*\right)}{\left(1+ACM_h^*\right)(j\omega)^2 + \left(\Lambda + C + ACD_h^*\right)(j\omega) + \left(\Lambda C + ACK_h^*\right)} \right\|_\infty \leq 1 \tag{92}$$

$$\left\| \frac{-ACM_e(j\omega)^2 + (C - ACD_e)(j\omega) + (C\Lambda - ACK_e)}{\left(1+ACM_e\right)(j\omega)^2 + (\Lambda + C + ACD_e)(j\omega) + (\Lambda C + ACK_e)} \right\|_\infty \leq 1. \tag{93}$$

To satisfy the stability conditions in (92) and (93), the following relation must be satisfied:

$$\begin{aligned}
&[(\Lambda C + ACK) - (1 + ACM)\omega^2]^2 \\
&\quad + [(\Lambda + C + ACD)\omega]^2 - [(C - ACD)\omega]^2 \\
&\quad - [(\Lambda C - ACK) + ACM\omega^2]^2 \geq 0
\end{aligned} \tag{94}$$

for both the slave and master manipulators by substituting M, D, and K with M_e, D_e, and K_e (the slave side), or M_h^*, D_h^*, and K_h^* (the master side), respectively. Furthermore, to satisfy (94),

$$\mathbf{a}\omega^4 + \mathbf{b}\omega^2 + \mathbf{c} \geq 0 \tag{95}$$

This article has been accepted for inclusion in a future issue of this journal. Content is final as presented, with the exception of pagination.

must hold, where

$$\begin{cases} \mathbf{a} = 1 + 2ACM \\ \mathbf{b} = \Lambda^2 + 2AC(2ACD - K - 2\Lambda ACM) \\ \mathbf{c} = 4\Lambda AC^2 K. \end{cases} \tag{96}$$

It follows directly from the positive-definite properties of M, D, K, C, and Λ that $\mathbf{a} \geq 0$ and $\mathbf{c} > 0$ hold indefinitely. Consequently, it follows from (94)–(96) that

$$\mathbf{b} + 4C\sqrt{\Lambda AK(2ACM + 1)} \geq 0 \tag{97}$$

must hold to fulfill the stability conditions in (92) and (93).

REFERENCES

[1] B. D. Argall, S. Chernova, M. Veloso, and B. Browning, "A survey of robot learning from demonstration," *Robot. Auto. Syst.*, vol. 57, no. 5, pp. 469–483, May 2009.

[2] M. Suomalainen, J. Koivumaki, S. Lampinen, V. Kyrki, and J. Mattila, "Learning from demonstration for hydraulic manipulators," in *Proc. IEEE/RSJ Int. Conf. Intell. Robots Syst. (IROS)*, Oct. 2018, pp. 3579–3586.

[3] A. Pervez, A. Ali, J.-H. Ryu, and D. Lee, "Novel learning from demonstration approach for repetitive teleoperation tasks," in *Proc. IEEE World Haptics Conf. (WHC)*, Jun. 2017, pp. 60–65.

[4] I. Havoutis and S. Calinon, "Learning from demonstration for semi-autonomous teleoperation," *Auto. Robots*, vol. 43, no. 3, pp. 713–726, Mar. 2019.

[5] J. Mattila, J. Koivumäki, D. G. Caldwell, and C. Semini, "A survey on control of hydraulic robotic manipulators with projection to future trends," *IEEE/ASME Trans. Mechatronics*, vol. 22, no. 2, pp. 669–680, Apr. 2017.

[6] J. Koivumaki and J. Mattila, "Stability-guaranteed force-sensorless contact force/motion control of heavy-duty hydraulic manipulators," *IEEE Trans. Robot.*, vol. 31, no. 4, pp. 918–935, Aug. 2015.

[7] P. F. Hokayem and M. W. Spong, "Bilateral teleoperation: An historical survey," *Automatica*, vol. 42, no. 12, pp. 2035–2057, Dec. 2006.

[8] M. Ostoja-Starzewski and M. Skibniewski, "A master-slave manipulator for excavation and construction tasks," *Robot. Auto. Syst.*, vol. 4, no. 4, pp. 333–337, Apr. 1989.

[9] S. Salcudean, K. Hashtrudi-Zaad, S. Tafazoli, S. P. DiMaio, and C. Reboulet, "Bilateral matched-impedance teleoperation with application to excavator control," *IEEE Control Syst.*, vol. 19, no. 6, pp. 29–37, Dec. 1999.

[10] S. Tafazoli, S. E. Salcudean, K. Hashtrudi-Zaad, and P. D. Lawrence, "Impedance control of a teleoperated excavator," *IEEE Trans. Control Syst. Technol.*, vol. 10, no. 3, pp. 355–367, May 2002.

[11] J. Koivumaki and J. Mattila, "Stability-guaranteed impedance control of hydraulic robotic manipulators," *IEEE/ASME Trans. Mechatronics*, vol. 22, no. 2, pp. 601–612, Apr. 2017.

[12] J. Koivumäki, W.-H. Zhu, and J. Mattila, "Energy-efficient and high-precision control of hydraulic robots," *Control Eng. Pract.*, vol. 85, pp. 176–193, Apr. 2019.

[13] D.-H. Zhai and Y. Xia, "A novel switching-based control framework for improved task performance in teleoperation system with asymmetric time-varying delays," *IEEE Trans. Cybern.*, vol. 48, no. 2, pp. 625–638, Feb. 2018.

[14] A. Aijaz, M. Dohler, A. H. Aghvami, V. Friderikos, and M. Frodigh, "Realizing the tactile Internet: Haptic communications over next generation 5G cellular networks," *IEEE Wireless Commun.*, vol. 24, no. 2, pp. 82–89, Apr. 2017.

[15] J. Guo, C. Liu, and P. Poignet, "A scaled bilateral teleoperation system for robotic-assisted surgery with time delay," *J. Intell. Robotic Syst.*, vol. 95, no. 1, pp. 165–192, Aug. 2018.

[16] P. Malysz and S. Sirouspour, "A kinematic control framework for single-slave asymmetric teleoperation systems," *IEEE Trans. Robot.*, vol. 27, no. 5, pp. 901–917, Oct. 2011.

[17] A. Shahdi and S. Sirouspour, "Adaptive/robust control for time-delay teleoperation," *IEEE Trans. Robot.*, vol. 25, no. 1, pp. 196–205, Feb. 2009.

[18] S. Sirouspour, "Modeling and control of cooperative teleoperation systems," *IEEE Trans. Robot.*, vol. 21, no. 6, pp. 1220–1225, Dec. 2005.

[19] Z. Chen, F. Huang, C. Yang, and B. Yao, "Adaptive fuzzy backstepping control for stable nonlinear bilateral teleoperation manipulators with enhanced transparency performance," *IEEE Trans. Ind. Electron.*, vol. 67, no. 1, pp. 746–756, Jan. 2020.

[20] D. Sun and Q. Liao, "Asymmetric bilateral telerobotic system with shared autonomy control," *IEEE Trans. Control Syst. Technol.*, early access, Sep. 23, 2020, doi: 10.1109/TCST.2020.3018426.

[21] A. Muhammad *et al.*, "Development of water hydraulic remote handling system for divertor maintenance of ITER," in *Proc. IEEE 22nd Symp. Fusion Eng.*, Jun. 2007, pp. 1–4.

[22] S. E. Salcudean and W.-H. Zhu, "Stability guaranteed teleoperation: An adaptive motion/force control approach," *IEEE Trans. Autom. Control*, vol. 45, no. 11, pp. 1951–1969, Nov. 2000.

[23] S. Lampinen, J. Koivumäki, and J. Mattila, "Full-dynamics-based bilateral teleoperation of hydraulic robotic manipulators," in *Proc. IEEE 14th Int. Conf. Autom. Sci. Eng. (CASE)*, Aug. 2018, pp. 1343–1350.

[24] S. Lampinen, J. Koivumäki, and J. Mattila, "Bilateral teleoperation of a hydraulic robotic manipulator in contact with physical and virtual constraints," in *Proc. BATH/ASME Symp. Fluid Power Motion Control*, 2018.

[25] S. Mastellone and A. van Delft, "The impact of control research on industrial innovation: What would it take to make it happen?" *Control Eng. Pract.*, vol. 111, Jun. 2021, Art. no. 104737.

[26] S. Lampinen, J. Koivumäki, and J. Mattila, "Bilateral teleoperation of a hydraulic robotic manipulator in contact with physical and virtual constraints," in *Proc. BATH/ASME Symp. Fluid Power Motion Control*. Fluid Power Systems Technology, Sep. 2018, Art. no. V001T01A021. [Online]. Available: https://asmedigitalcollection.asme.org/FPST/proceedings-pdf/FPMC2018/51968/V001T01A021/2388188/v001t01a021-fpmc2018-8842.pdf, doi: 10.1115/FPMC2018-8842.

[27] W.-H. Zhu, Y.-G. Xi, Z.-J. Zhang, Z. Bien, and J. De Schutter, "Virtual decomposition based control for generalized high dimensional robotic systems with complicated structure," *IEEE Trans. Robot. Autom.*, vol. 13, no. 3, pp. 411–436, Jun. 1997.

[28] W.-H. Zhu, T. Lamarche, E. Dupuis, D. Jameux, P. Barnard, and G. Liu, "Precision control of modular robot manipulators: The VDC approach with embedded FPGA," *IEEE Trans. Robot.*, vol. 29, no. 5, pp. 1162–1179, Oct. 2013.

[29] W.-H. Zhu, "Dynamics of general constrained robots derived from rigid bodies," *J. Appl. Mech.*, vol. 75, no. 3, pp. 031005-1–031005-11, May 2008.

[30] H. Kazerooni and M.-G. Her, "The dynamics and control of a haptic interface device," *IEEE Trans. Robot. Autom.*, vol. 10, no. 4, pp. 453–464, Aug. 1994.

[31] J. D. Cooke, "Dependence of human arm movements on limb mechanical properties," *Brain Res.*, vol. 165, no. 2, pp. 366–369, Apr. 1979.

[32] P. Malysz and S. Sirouspour, "Nonlinear and filtered force/position mappings in bilateral teleoperation with application to enhanced stiffness discrimination," *IEEE Trans. Robot.*, vol. 25, no. 5, pp. 1134–1149, Oct. 2009.

[33] T. Hu, J. Kühn, and S. Haddadin, "Forward and inverse dynamics modeling of human shoulder-arm musculoskeletal system with scapulothoracic constraint," *Comput. Methods Biomech. Biomed. Eng.*, vol. 23, no. 11, pp. 785–803, Aug. 2020.

[34] S. Haddadin, A. De Luca, and A. Albu-Schaffer, "Robot collisions: A survey on detection, isolation, and identification," *IEEE Trans. Robot.*, vol. 33, no. 6, pp. 1292–1312, Dec. 2017.

[35] J. Koivumäki and J. Mattila, "Adaptive and nonlinear control of discharge pressure for variable displacement axial piston pumps," *J. Dyn. Syst., Meas., Control*, vol. 139, no. 10, Oct. 2017.

[36] G. Tao, "A simple alternative to the Barbalat lemma," *IEEE Trans. Autom. Control*, vol. 42, no. 5, p. 698, May 1997.

Santeri Lampinen received the bachelor's and M.Sc. degrees (Hons.) in machine automation from the Tampere University of Technology, Tampere, Finland, in 2017 and 2018, respectively.

He has been working with the Tampere University of Technology since 2017 and since 2018 he has been pursuing doctoral degree in machine automation. His research interests include mining automation, control of teleoperation systems, control of hydraulic systems, and nonlinear-model-based control.

This article has been accepted for inclusion in a future issue of this journal. Content is final as presented, with the exception of pagination.

Janne Koivumäki (Member, IEEE) received the M.Sc. degree in automation engineering and the Dr.Tech. degree in automation science and engineering from the Tampere University of Technology, Tampere, Finland, in 2012 and 2016, respectively.

From 2011 to 2019, he worked with the Department of Intelligent Hydraulics and Automation, Tampere University of Technology. In 2019, he joined the Novatron Oy, Pirkkala, Finland, where he currently works as a Robotics and Control Systems Scientist. His research interests include an earth-moving automation, hydraulic robotic manipulators, constrained motion control, and energy efficiency.

Wen-Hong Zhu (Senior Member, IEEE) received the bachelor's and M.S. degrees from Northwestern Polytechnical University, Xi'an, China, in 1984 and 1987, respectively, and the Ph.D. degree from Xi'an Jiaotong University, Xi'an, in 1991.

He was a Post-Doctoral Fellow with Shanghai Jiao Tong University, Shanghai, China, during 1991–1993; the Korea Advanced Institute of Science and Technology, Daejeon, Korea, in 1995; Katholieke Universiteit Leuven, Leuven, Belgium, during 1996–1997; and the University of British Columbia, Vancouver, BC, Canada, during 1997–1999. He was with the University of British Columbia as a Scientific Engineer from 1999 to 2001 until he joined the Canadian Space Agency (CSA), Saint-Hubert, QC, Canada, as an engineering employee. He is the initiator of Virtual Decomposition Control.

Jouni Mattila (Member, IEEE) received the M.Sc. and Ph.D. degrees in automation engineering, both from the Tampere University of Technology, Tampere, Finland, in 1995 and 2000, respectively.

He is currently a Professor of machine automation with the unit of Automation Technology and Mechanical Engineering, Tampere University. His research interests include machine automation, nonlinear model-based control of robotic manipulators, and energy-efficient control of heavy-duty robotic systems.